

Application of the Transmission-Line Matrix Method to Open Region Field Problems

by

Neil R. S. Simons

A thesis
presented to the University of Manitoba
in partial fulfillment of the
requirements for the degree of
Master of Science
in
Electrical Engineering

Winnipeg, Manitoba, 1989
© Neil R. S. Simons, 1989



National Library
of Canada

Bibliothèque nationale
du Canada

Canadian Theses Service Service des thèses canadiennes

Ottawa, Canada
K1A 0N4

The author has granted an irrevocable non-exclusive licence allowing the National Library of Canada to reproduce, loan, distribute or sell copies of his/her thesis by any means and in any form or format; making this thesis available to interested persons.

The author retains ownership of the copyright in his/her thesis. Neither the thesis nor substantial extracts from it may be printed or otherwise reproduced without his/her permission.

L'auteur a accordé une licence irrévocable et non exclusive permettant à la Bibliothèque nationale du Canada de reproduire, prêter, distribuer ou vendre des copies de sa thèse de quelque manière et sous quelque forme que ce soit pour mettre des exemplaires de cette thèse à la disposition des personnes intéressées.

L'auteur conserve la propriété du droit d'auteur qui protège sa thèse. Ni la thèse ni des extraits substantiels de celle-ci ne doivent être imprimés ou autrement reproduits sans son autorisation.

ISBN 0-315-63340-9

Canada

APPLICATION OF THE TRANSMISSION-LINE MATRIX
METHOD TO OPEN REGION FIELD PROBLEMS

BY

NEIL R.S. SIMONS

A thesis submitted to the Faculty of Graduate Studies of
the University of Manitoba in partial fulfillment of the requirements
of the degree of

MASTER OF SCIENCE

© 1990

Permission has been granted to the LIBRARY OF THE UNIVERSITY OF MANITOBA to lend or sell copies of this thesis. to the NATIONAL LIBRARY OF CANADA to microfilm this thesis and to lend or sell copies of the film, and UNIVERSITY MICROFILMS to publish an abstract of this thesis.

The author reserves other publication rights, and neither the thesis nor extensive extracts from it may be printed or otherwise reproduced without the author's written permission.

Abstract

In this thesis the application of the Transmission-Line Matrix (TLM) method to two dimensional scattering problems is investigated. The method is recognized as an efficient tool for the analysis of closed structures, since a single simulation using pulse excitation and Fourier transformations can produce accurate frequency domain results over a wide bandwidth. The Finite Difference-Time Domain (FD-TD) method is also a numerical method capable of simulating Maxwell's equations in space and time. The FD-TD method has been applied to the analysis of scattering simulations, however sinusoidal excitation has been used to obtain results at a single frequency. Both the TLM and FD-TD method require discretization of the entire simulation space, and therefore require special treatment of artificial boundaries which are applied to limit the simulation space to a computationally acceptable size. The relationship between the TLM and FD-TD methods was extensively investigated in two dimensions.

Software capable of modelling arbitrarily shaped scatterers was written to perform the simulations. To illuminate the scatterer with an accurate incident field and apply absorbing boundary conditions to only the scattered field, a method (that has been used extensively with the FD-TD method) was formulated in terms of a time domain equivalence principle for the excitation of electrical networks in order to implement the method into TLM programs. Fourier transformation of time domain results was found to be extremely sensitive to numerical errors, such as those produced by inaccurate absorbing boundary conditions. Previous methods of match terminating the TLM mesh were found to be inaccurate for the application considered in this thesis. The absorbing boundary conditions used in this thesis were originally derived for use with finite difference approximations of the wave equation. Using the relationship established between the FD-TD and TLM methods, these boundary conditions were applied to the TLM method.

Scattered far field patterns were calculated for a perfectly conducting square cylinder, a perfectly conducting circular cylinder, and a perfectly conducting strip (for both broad side and edge incidence). The TLM results for each geometry are compared to established solutions over a wide range of frequencies. For the square cylinder, accurate results (compared to Boundary Element Method (BEM) results using an error norm) are obtained over a range $ka=0.3$ to 8. For the circular cylinder accurate results (compared to an analytical solution using an error norm) are obtained over a range

$ka=0.3$ to 6.

As the geometrical complexity of a scatterer increases, the FD-TD method using sinusoidal excitation becomes more efficient than using integral equation techniques. In this thesis, it is demonstrated that for scatterers with simple geometries (handled efficiently by integral equation techniques), the TLM method using pulse excitation and Fourier transformations to obtain frequency domain results, becomes more efficient than integral equation techniques as the number of frequency points is increased.

Acknowledgments

I would like to thank Professor E. Bridges for his supervision, encouragement and guidance throughout the course of this work.

I would also like to acknowledge: Walid Shamma for many helpful discussions regarding the FD-TD method, Blake Podaima for invaluable assistance in producing this document, Neil Aitken of Quantic Laboratories for assistance in developing the Boundary Element program used as a verification tool in this thesis, and David Roscoe, Roger Toutant, Vladimir Labay, and Marc Opie for many helpful discussions.

Financial support from the Natural Sciences and Engineering Research Council of Canada is acknowledged.

Table of Contents

Abstract	ii
Acknowledgements	iv
Table of Contents	v
List of Figures	ix
List of Tables	xiv
Chapter 1: Introduction	1
Chapter 2: Review of the Transmission-Line Matrix Method	4
2.1. Transmission-Line Matrix Theory	4
2.1.1. Lumped Element Model of Maxwell's Equations	4
2.1.2. Derivation of the Transmission Line Model	9
2.1.3. Two Dimensional Series Node	14
2.1.4. Representation of an Arbitrary Medium with a Transmission Line Model	16
2.1.5. Three Dimensional TLM	20
2.2. Computer Simulation of the Transmission Line Network	22
2.2.1. Algorithm	23
2.2.2. Boundary Conditions	27
2.2.3. Obtaining Frequency Domain Results from a Time Domain Simulation	31
2.3. Errors in TLM Simulations and their Correction	31
2.3.1. Truncation Error	32
2.3.2. Velocity Error	32
2.3.3. Coarseness Error	33

2.4. Applications of the TLM Method	33
2.4.1. TLM and Open Region Problems	34
Chapter 3: Comparison of TLM and Similar Methods	37
3.1. Comparison of TLM and FD-TD	38
3.1.1. Previous Comparisons of TLM and FD-TD	38
3.1.2. Comparison of Time Stepping Procedures	39
3.1.2.1. Review of the FD-TD Method	40
3.1.2.2. Modified TLM Scheme	43
3.1.2.3. Equivalence of Modified TLM and FD-TD	47
3.1.3. Comparison By Propagation Analysis	51
3.1.3.1. Dispersion Relation of FD-TD Method	52
3.1.3.2. Propagation Analysis of the TLM Node	54
3.1.3.3. Equivalence of Propagation Characteristics	57
3.2. TLM and Berenger's Method	59
Chapter 4: Application of the TLM Method to Scattering Problems	63
4.1. Configuration of the Mesh	64
4.1.1. Time Domain Equivalence Principle	66
4.1.2. Use of Equivalent Excitation in TLM Simulations	70
4.2. Absorbing Boundary Conditions	74
4.2.1. Match Termination of a TLM Mesh	75
4.2.2. Implementation of the Variable Impedance Boundary Condition	79
4.2.3. FD-TD Absorbing Boundary Conditions	80
4.2.4. Higdon's Absorbing Boundary Conditions	82
4.2.4.1. General Formulation	82
4.2.4.2. Stability and Accuracy	84

4.2.4.3. Application of Higdon's Conditions to TLM Simulations	86
4.3. Calculation of Far Field Patterns	89
4.3.1. Surface Current to Far Field Transformation	89
4.3.2. Near Field to Far Field Transformation	91
4.3.3. Direct Transformation to the Far Field in the Time Domain	92
4.3.3. Calculation of Frequency Domain Scattered Fields from Time Domain Field Simulations	92
Chapter 5: Software Validation and Testing	95
5.1. Validation of the Time Domain Equivalence Principle	95
5.2. Testing of the Absorbing Boundary Conditions	102
5.2.1. Normal Incidence	103
5.2.2. Arbitrary Incidence	107
5.3. Software	118
5.3.1. TLM_scatt	118
5.3.2. Calculation of Scattered Far Field Patterns	127
Chapter 6: Results	129
6.1. Perfectly Conducting Rectangular Cylinder	129
6.2. Perfectly Conducting Circular Cylinder	141
6.3. Perfectly Conducting Strip	150
6.4. Accuracy and Efficiency of TLM Scattering Simulations	154
6.4.1. Comparison of Pulse and Sinusoidal Excitation	154

6.4.2. Comparison of the Efficiency of TLM and Integral Equation Methods	159
Chapter 7: Conclusions and Future Research	163
7.1. Conclusions	163
7.2. Future Research	166
Appendix A: Time Domain Field Distributions	168
A.1. Perfectly Conducting Square Cylinder	169
A.2. Perfectly Conducting Circular Cylinder	172
A.3. Perfectly Conducting Infinitely Thin Strip (Broadside Incidence)	175
References	178

List of Figures

Figure 2.1: <i>Lumped network model of Maxwell's equations in two dimensions</i>	6
Figure 2.2: <i>Representation of the lumped element node as the intersection of two identical circuits</i>	10
Figure 2.3: <i>Equivalent-tee lumped element network representation for a transmission line</i>	11
Figure 2.4: <i>The two dimensional TLM shunt node</i>	12
Figure 2.5: <i>The two dimensional TLM series node</i>	15
Figure 2.6: <i>Two dimensional TLM shunt node for arbitrary media properties</i>	18
Figure 2.7: <i>Three dimensional expanded node</i>	21
Figure 2.8: <i>Three dimensional symmetric condensed node</i>	22
Figure 2.9: <i>Scattering of a unit magnitude impulse off a two dimensional shunt node</i>	24
Figure 2.10: <i>Propagation of an impulsive disturbance through a mesh of shunt nodes</i>	26
Figure 2.11: <i>Modelling of a curved boundary with a rectangular TLM mesh</i>	30
Figure 3.1: <i>Physical layout of field quantities on a FD-TD grid</i>	41
Figure 3.2: <i>Operation of five TLM nodes through one time</i>	46
Figure 3.3: <i>Operation of two nodes adjacent in the y direction</i>	49
Figure 3.4: <i>Equivalent circuit of TLM shunt node loaded with permittivity and loss stubs with three branches terminated in a short circuit</i>	55
Figure 3.5: <i>Dispersion characteristics of a transmission line and lumped element network for diagonal propagation</i>	61
Figure 3.6: <i>Dispersion characteristics of a transmission line and lumped element network for axial propagation</i>	61
Figure 4.1: <i>Two dimensional scattering problem</i>	65

Figure 4.2: <i>Electrical network used to formulate the time domain equivalence principle</i>	67
Figure 4.3: <i>Equivalent excitation of an electrical network</i>	69
Figure 4.4: <i>TLM simulation of a plane wave propagating through free space</i>	71
Figure 4.5: <i>TLM simulation space used to model two dimensional scattering problems</i>	72
Figure 4.6: <i>E-polarized plane wave</i>	77
Figure 4.7: <i>TLM simulation space used to model two dimensional scattering problems</i>	91
Figure 5.1: <i>Mesh used to test the one dimensional total scattered field formulation</i>	96
Figure 5.2: <i>Frequency domain results obtained from the one dimensional tests of the total scattered field formulation (match termination)</i>	98
Figure 5.3: <i>Frequency domain results obtained from the one dimensional tests of the total scattered field formulation (short circuit termination)</i>	99
Figure 5.4: <i>Equivalent excitation of the total field region without a scatterer present</i>	101
Figure 5.5: <i>Mesh used to test the the absorbing boundary for normal incidence</i>	104
Figure 5.6: <i>Snapshots of the electric field distribution for plane wave excitation</i>	105
Figure 5.7: <i>Mesh used to test the absorbing boundary conditions for arbitrary incidence</i>	108
Figure 5.8: <i>Time domain response obtained at output point 1, (a) comparing match termination for normal incidence and first order averaging to the benchmark solution and, (b) comparing match termination for normal incidence and second order averaging to the benchmark solution</i>	109
Figure 5.9: <i>Time domain response obtained at output point 1, comparison of first and second order averaging to first and second order space time extrapolation</i>	111

Figure 5.10: Time domain response obtained at output point 2, (a) match termination for normal incidence and first order averaging compared to the benchmark solution, (b) match termination for normal incidence and second order averaging compared to the benchmark solution	112
Figure 5.11: Time domain response obtained at output point 3, (a) match termination for normal incidence and first order averaging compared to the benchmark solution, (b) match termination for normal incidence and second order averaging compared to the benchmark solution	114
Figure 5.12: Time domain response obtained at output point 4, (a) match termination for normal incidence and first order averaging compared to the benchmark solution, (b) match termination for normal incidence and second order averaging compared to the benchmark solution	115
Figure 5.13: Time domain response obtained at output point 2, comparing third order space time extrapolation to the benchmark solution	117
Figure 5.14: Time domain response obtained at output point 2, comparing third order space time extrapolation, second order averaging, and match termination for normal incidence to the benchmark solution	118
Figure 5.15: (a) Flowchart of a typical TLM program, Fourier transforms are performed after the iteration process (b) Flowchart of a modified TLM program, Fourier transforms are performed during the iteration process	124
Figure 5.16: Flowchart of TLM_scatt	126
Figure 6.1: Simulation space used to analyze a perfectly conducting square cylinder	130
Figure 6.2: Frequency domain scattered far field pattern for a perfectly conducting square cylinder, $ka=0.2$	132
Figure 6.3: Frequency domain scattered far field pattern for a perfectly conducting square cylinder, $ka=0.4$	132
Figure 6.4: Frequency domain scattered far field pattern for a perfectly conducting square cylinder, $ka=0.6$	133
Figure 6.5: Frequency domain scattered far field pattern for a perfectly conducting square cylinder, $ka=0.8$	133
Figure 6.6: Frequency domain scattered far field pattern for a perfectly conducting square cylinder, $ka=4.0$	134
Figure 6.7: Frequency domain scattered far field pattern for a perfectly conducting square cylinder, $ka=6.0$	134

Figure 6.8: <i>Frequency domain scattered far field pattern for a perfectly conducting square cylinder, $ka=8.0$</i>	135
Figure 6.9: <i>Frequency domain scattered far field pattern for a perfectly conducting square cylinder, $ka=10.0$</i>	135
Figure 6.10: <i>Frequency domain scattered far field pattern for a perfectly conducting square cylinder, $ka=0.8$ (polar coordinates)</i>	136
Figure 6.11: <i>Frequency domain scattered far field pattern for a perfectly conducting square cylinder, $ka=6.0$ (polar coordinates)</i>	136
Figure 6.12: <i>Error norm versus ka for a perfectly conducting square cylinder</i>	139
Figure 6.13: <i>Error norm versus ka for a perfectly conducting square cylinder, with first order boundary conditions used to truncate the scattered field region</i>	140
Figure 6.14: <i>Simulation space used to analyze a perfectly conducting circular cylinder</i>	141
Figure 6.15: <i>Frequency domain scattered far field pattern for a perfectly conducting circular cylinder, $ka=0.2$</i>	143
Figure 6.16: <i>Frequency domain scattered far field pattern for a perfectly conducting circular cylinder, $ka=0.4$</i>	143
Figure 6.17: <i>Frequency domain scattered far field pattern for a perfectly conducting circular cylinder, $ka=0.6$</i>	144
Figure 6.18: <i>Frequency domain scattered far field pattern for a perfectly conducting circular cylinder, $ka=0.8$</i>	144
Figure 6.19: <i>Frequency domain scattered far field pattern for a perfectly conducting circular cylinder, $ka=4.0$</i>	145
Figure 6.20: <i>Frequency domain scattered far field pattern for a perfectly conducting circular cylinder, $ka=6.0$</i>	145
Figure 6.21: <i>Frequency domain scattered far field pattern for a perfectly conducting circular cylinder, $ka=8.0$</i>	146
Figure 6.22: <i>Frequency domain scattered far field pattern for a perfectly conducting circular cylinder, $ka=10.0$</i>	146
Figure 6.23: <i>Frequency domain scattered far field pattern for a perfectly conducting circular cylinder, $ka=0.8$ (polar coordinates)</i>	147

Figure 6.24: <i>Frequency domain scattered far field pattern for a perfectly conducting circular cylinder, $ka=6.0$ (polar coordinates)</i>	147
Figure 6.25: <i>Error norm versus ka for a perfectly conducting circular cylinder</i>	149
Figure 6.26: <i>Simulation space used to analyze a perfectly conducting thin strip for broadside incidence</i>	150
Figure 6.27: <i>Comparison of TLM results and an analytical solution for the case of a perfectly conducting thin strip with broadside incidence for $ka=1.0$</i>	152
Figure 6.28: <i>Comparison of TLM results and an analytical solution for the case of a perfectly conducting thin strip with broadside incidence for $ka=5.0$</i>	152
Figure 6.29: <i>Comparison of TLM results and an analytical solution for the case of a perfectly conducting thin strip with edge incidence for $ka=1.0$</i>	153
Figure 6.30: <i>Comparison of TLM results and an analytical solution for the case of a perfectly conducting thin strip with edge incidence for $ka=5.0$</i>	153
Figure 6.31: <i>Comparison of TLM and BEM far field patterns for a perfectly conducting square cylinder, for $ka= 0.6$ and 1.0</i>	155
Figure 6.32: <i>cpu time required by the TLM and BEM programs versus the number of output frequency points</i>	162
Figure A.1: <i>Time domain field distributions for a perfectly conducting square cylinder</i>	169
Figure A.2: <i>Time domain field distributions for a perfectly conducting circular cylinder</i>	172
Figure A.3: <i>Time domain field distributions for a perfectly conducting thin strip (broadside incidence)</i>	175

List of Tables

Table 4.1: <i>Peak to peak reflections caused by boundary conditions under normal incidence (in percent of the incident wave)</i>	106
--	-----

Chapter 1

Introduction

The Method of Moments (MoM) [1] has been used extensively to analyze electromagnetic field problems. Applying MoM to an electromagnetic field problem yields an approximate solution to an integral equation which governs the physical system being analyzed. The integral equation is formulated on the surfaces and media interfaces of the scatterer and therefore, only these surfaces require discretization. Because MoM provides a time harmonic solution, a single simulation yields results at one frequency.

The Finite Difference-Time Domain (FD-TD) method, originally proposed by Yee [2], applies central difference approximations to the time and spatial derivatives in Maxwell's equations. The FD-TD method, since it is based on an approximation to differential equations, requires discretization of the entire simulation space. The simulation of an open region problem implies that an infinite space is required. However, because computer resources are finite, artificial boundary conditions are applied to absorb outward travelling waves and truncate the simulation space to a reasonable size [3]. These artificial boundary conditions are called absorbing boundary conditions.

Taflove and Umashankar [4],[5] have applied the FD-TD method to the solution of electromagnetic scattering problems. Absorbing boundary conditions are used to limit the size of the simulation space, and accurate results at a single frequency have been obtained by exciting the mesh with a sinusoidal signal. Taflove and Umashankar [4] have argued that as the geometrical complexity of the material properties of a scatterer increases, the computational efficiency of the FD-TD method, despite the

large computer resource requirements, approaches that of MoM.

The Transmission-Line Matrix (TLM) method, originated by Johns and Beurle [6], is similar to the FD-TD method in that it provides an approximate solution to Maxwell's equations in the time domain, and requires discretization of the entire simulation space. The method is based on a lumped element model of Maxwell's equations from which a transmission line model is obtained. The method has been recognized as an efficient and accurate tool for the analysis of waveguides, finlines, and other closed structures [7]. Recently, the TLM method has been applied to model open structures [8], and many of the issues regarding the modelling of open region problems such as absorbing boundary conditions have not been resolved. The main advantage of using the TLM method is the amount of information that is available from a single simulation. By using a method that simulates Maxwell's equations in space and time, accurate frequency domain results can be obtained over a wide bandwidth from a single simulation using pulse excitation and Fourier transformation of the output impulse response. Because Taflove and Umashankar have used sinusoidal excitation rather than pulse excitation, their investigations have not taken full advantage of solving Maxwell's equations in the time domain. Accurate results have been obtained, but the full potential of time domain analysis has not been realized.

The purpose of this thesis is to investigate the application of the TLM method to two dimensional scattering problems. Topics associated with the modelling of open region problems are discussed. To achieve computational efficiency, the use of pulse excitation and Fourier transforms to obtain wide band frequency domain results from a single simulation is investigated.

Chapter 2 provides a review of the basic TLM method and a discussion of enhancements that have been developed over the past fifteen years. Also included is a review of previous attempts at applying the TLM method to open region problems.

Chapter 3 discusses the relationship between the TLM method and two other methods capable of simulating electromagnetic fields in the time domain, the FD-TD method and the Spatial Network Method (SNM). Establishing relationships between the TLM and similar methods will allow the transfer of compatible developments and enhancement of all relevant methods.

Application of the TLM method to scattering problems is discussed in chapter 4. To accurately model incident and scattered fields, a method that separates scattered fields from total fields is implemented. This scheme has been used in FD-TD programs and in chapter 4 is reformulated in terms of a time domain equivalence principle for implementation into TLM programs. A review of absorbing boundary conditions used with the FD-TD method is provided, and the application of two types of absorbing boundary conditions to TLM simulations is discussed. As well, a potentially accurate absorbing boundary condition applicable to the TLM method (the variable impedance boundary condition), is derived and discussed. Implementation at the time of writing this thesis has not been attempted.

In chapter 5, the developments presented in chapter 4 are tested. The total/scattered field formulation is tested for one and two dimensional simulations. The absorbing boundary conditions are tested and comparisons are made to the traditional method of match terminating a TLM mesh. A significant observation discussed in chapter 6 is that previous methods match terminating a TLM mesh are not accurate, therefore the implementation of the FD-TD absorbing boundary conditions is a significant step in improving TLM modelling of open region problems. A description of the software developed to model the two dimensional scattering problems considered in this thesis is also provided. Finally, chapter 7 will summarize the work presented in this thesis and topics of future research will be included.

Chapter 2

Review of the Transmission-Line Matrix Method

2.1. Transmission-Line Matrix Theory

2.1.1. Lumped Element Model of Maxwell's Equations

For a lossless space of permittivity ϵ and permeability μ , Maxwell's curl equations are

$$\nabla \times \mathbf{H} = \epsilon \frac{\partial \mathbf{E}}{\partial t} \quad (2.1a)$$

$$\nabla \times \mathbf{E} = -\mu \frac{\partial \mathbf{H}}{\partial t} \quad (2.1b)$$

If only two dimensional problems are considered with no variation in the z -direction, equations (2.1) yield two independent sets of equations. Equations (2.2) represent Maxwell's equations for two dimensional transverse electric (TE) propagation ($H_z = 0$),

$$\frac{\partial E_z}{\partial x} = \mu \frac{\partial H_y}{\partial t} \quad (2.2a)$$

$$\frac{\partial E_z}{\partial y} = -\mu \frac{\partial H_x}{\partial t} \quad (2.2b)$$

$$\frac{\partial H_y}{\partial x} - \frac{\partial H_x}{\partial y} = \epsilon \frac{\partial E_z}{\partial t} \quad (2.2c)$$

and equations (2.3) represent Maxwell's equations for two dimensional transverse

magnetic (TM) propagation ($E_z=0$).

$$-\frac{\partial H_z}{\partial x} = \epsilon \frac{\partial E_y}{\partial t} \quad (2.3a)$$

$$\frac{\partial H_z}{\partial y} = \epsilon \frac{\partial E_x}{\partial t} \quad (2.3b)$$

$$\frac{\partial E_y}{\partial x} - \frac{\partial E_x}{\partial y} = -\mu \frac{\partial H_z}{\partial t} \quad (2.3c)$$

Consider the lumped element network shown in Figure 2.1. The network lies in the x - y plane and is oriented as indicated in the figure. Spacing between the nodes in the network is Δl and the values of inductance and capacitance are $L\Delta l$ and $2C\Delta l$, respectively. This network was proposed as a model of Maxwell's equations in two dimensions by Gabriel Kron in 1943 [9]. To utilize the equivalent circuit in a practical sense, "network analyzers" were built consisting of meshes of inductors and capacitors [10]. With the appropriate excitation and boundary conditions applied to the mesh, a variety of electromagnetic field problems can be studied. Whinnery and Ramo used a network analyzer to study field distributions in cylindrical waveguides and the effects of discontinuities in rectangular waveguides [11]. Whinnery, Concordia, Ridgeway, and Kron examined field distributions in rectangular cavities of different shapes [12]. This technique yielded acceptable results considering the large amount of experimental error involved. An interesting account of the various problems associated with building a network analyzer can be found in a paper by Spangenberg, Walters, and Schott [10].

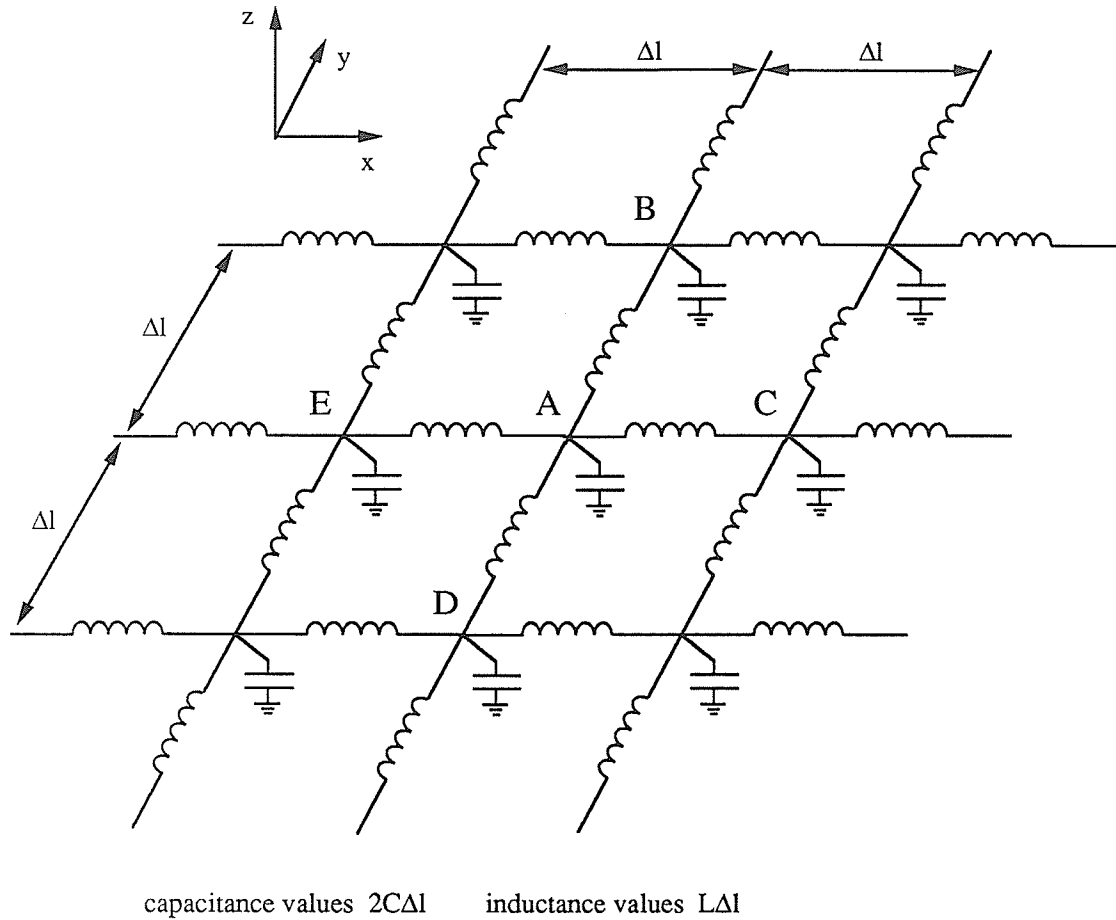


Figure 2.1: Lumped network model of Maxwell's equations in two dimensions proposed by Gabriel Kron [9].

Kron derived equivalent circuits to model various physical systems and established basic theory related to the construction of circuit models of differential equations [13]. Three dimensional models of Maxwell's equations were also derived, however only the two dimensional models were used in practice. The three dimensional networks contained ideal transformers and dependent voltage sources making

construction of a practical network difficult [14]. Recently, Johns has investigated the role of these components and determined that they are related to gauge transformations of Maxwell's equations [15]. Under certain circumstances the ideal transformers and dependent sources are not required. Johns derived lumped element models which satisfy the Coulomb and Lorentz gauges. Johns' paper, although theoretical (no one would consider actually building an equivalent network today), provides insight into lumped element modelling and the theory behind the models.

The analogy between Maxwell's equations and the equivalent network can be obtained by using simple circuit theory. In Figure 2.1, the voltage drop between nodes C and A can be expressed as

$$v_C - v_A = L \Delta l \frac{\partial i_{CA}}{\partial t} \quad (2.4)$$

where i_{CA} is the current flowing from node C to node A (in the negative x direction), v_A is the voltage at node A, and v_C is the voltage at node C. Equation (2.4) can be written for an arbitrary voltage drop across two adjacent nodes in the x direction.

$$\frac{v(x+\Delta l) - v(x)}{\Delta l} = -L \frac{\partial i_x}{\partial t} \quad (2.5)$$

Similarly, equation (2.6) is valid for an arbitrary voltage drop across two adjacent nodes in the y direction.

$$\frac{v(y+\Delta l) - v(y)}{\Delta l} = -L \frac{\partial i_y}{\partial t} \quad (2.6)$$

Applying Kirchoff's current law to node A yields

$$i_{EA} + i_{BA} + i_{CA} + i_{DA} = 2C \Delta l \frac{\partial v_A}{\partial t} \quad (2.7)$$

where i_{EA} and i_{CA} represent currents flowing in the positive and negative x directions respectively; and i_{DA} and i_{BA} represent currents flowing in the positive and negative y

directions respectively. If these currents are considered to be centered at locations half way between nodes, equation (2.7) can be written as,

$$i_x(x-\Delta l/2) - i_y(y+\Delta l/2) - i_x(x+\Delta l/2) + i_y(y-\Delta l/2) = 2C \Delta l \frac{\partial v_A}{\partial t} \quad (2.8)$$

or

$$-\frac{i_x(x+\Delta l/2) - i_x(x-\Delta l/2)}{\Delta l} - \frac{i_y(y+\Delta l/2) - i_y(y-\Delta l/2)}{\Delta l} = 2C \frac{\partial v_A}{\partial t} \quad (2.9)$$

Recognizing the left hand sides of equations (2.5), (2.6), and (2.9) as simple difference approximations to continuous derivatives, the network can be considered to be an approximation to the equations

$$\frac{\partial v}{\partial y} = -L \frac{\partial i_y}{\partial t} \quad (2.10a)$$

$$\frac{\partial v}{\partial x} = -L \frac{\partial i_x}{\partial t} \quad (2.10b)$$

$$-\frac{\partial i_x}{\partial x} - \frac{\partial i_y}{\partial y} = 2C \frac{\partial v}{\partial t} \quad (2.10c)$$

Examining the set of equations (2.10) modelled by the network and the set of Maxwell's equations for two dimensional TE propagation (2.2), the following set of relationships between field quantities in Maxwell's equations and circuit quantities in the lumped network of Figure 2.1 can be established;

$$E_z = v$$

$$H_y = -i_x$$

$$H_x = i_y$$

$$\text{and } \mu = L, \quad \epsilon = 2C \quad (2.11)$$

A similar equivalence between equations (2.10) and Maxwell's equations for two dimensional TM propagation (2.3) can be established

$$\begin{aligned}H_z &= v \\E_y &= i_x \\E_x &= -i_y\end{aligned}$$

and $\mu = 2C$, $\varepsilon = L$ (2.12)

A review of lumped element modelling as an experimental technique for solving electromagnetic field problems can be found in a book by D. Vitkovitch [16]. In modern engineering practice, lumped element modelling is no longer used as an experimental method. However, the concepts are important to numerical techniques which are based upon the lumped element models.

2.1.2. Derivation of the Transmission Line Model

Three possible approaches exist when solving electromagnetic field problems using lumped element models and the equivalence to Maxwell's equations.

- 1) The models could be built and measurements performed directly on the network.
- 2) The equivalent circuit model could be simulated directly using a circuit analysis tool specially adapted to take into account the nature of the network.
- 3) A new model could be constructed from the circuit model from which possible advantages could be realized.

As mentioned in the previous section, the first approach is unlikely considering the problems associated with building an experimental mesh, the inflexibility of having a physical model, and the errors involved in performing measurements on the model. The second and third approaches are more likely because of the flexibility and power of computer simulation. Yoshida and Fukai have developed a three dimensional numerical technique which simulates the lumped element network model of Maxwell's equations [17].

The TLM method is derived by proceeding with the third approach. The lumped element network of Figure 2.1 can be divided into individual building blocks from which an entire network can be constructed. The building block is shown in Figure 2.2(a) and can be considered as the intersection of two identical circuits as shown in Figure 2.2(b). Note the two lumped capacitances of $C\Delta l$ in Figure 2.2(b) combine to yield the $2C\Delta l$ capacitance in Figure 2.2(a). The individual circuits in Figure 2.2(b) are recognized as the equivalent tee network representation for a transmission line with distributed inductance L , and distributed capacitance C [18] (see Figure 2.3).

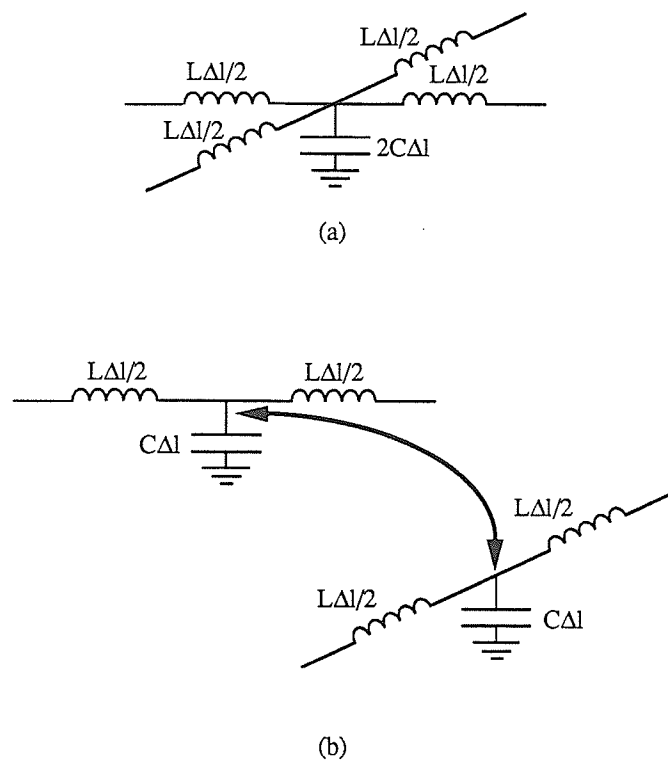


Figure 2.2: (a) The lumped element node (b) Representation as the intersection of two identical circuits

The intrinsic impedance of the transmission line is

$$Z = \sqrt{\frac{L}{C}} \quad (2.13)$$

and the speed of propagation along the line is

$$v = \frac{1}{\sqrt{LC}} \quad (2.14)$$

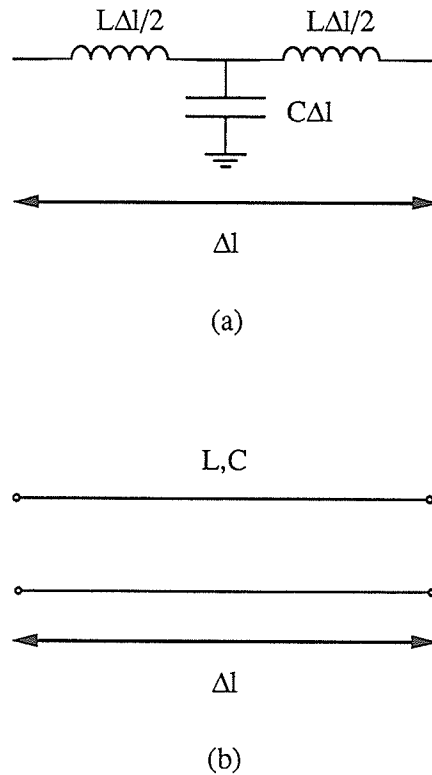


Figure 2.3: Equivalent-tee lumped element network representation for a transmission line [18].

The circuit of Figure 2.2(a) is considered as a lumped element representation of the intersection of two transmission lines shown in Figure 2.4. This simple transmission line network is referred to as the TLM shunt node and is the building block from

which an entire TLM mesh can be constructed. The intersecting transmission lines in Figure 2.4 are realized as two wire transmission lines and referred to as the elemental transmission lines of the model.

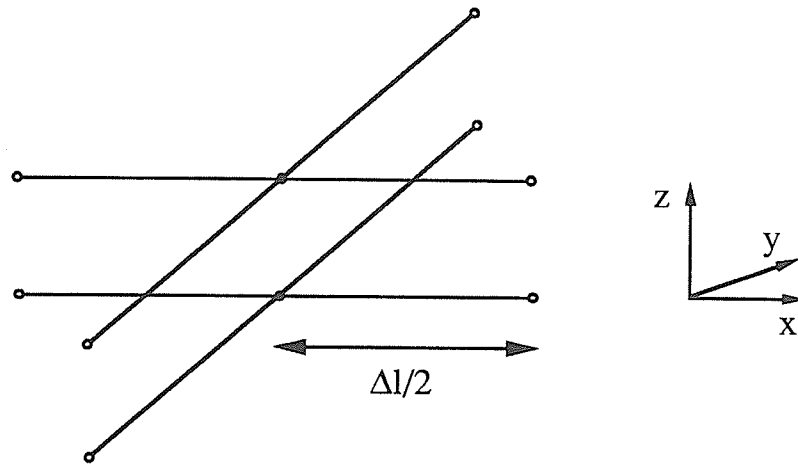


Figure 2.4: The two dimensional TLM shunt node represented as the shunt connection of two wire transmission lines.

The elemental transmission lines of the model are considered to represent free space ($L = \mu_o, C = \epsilon_o$). The velocity of propagation on the elemental transmission lines is

$$v_{\text{elemental line}} = \frac{1}{\sqrt{LC}} = c_o = 2.984 \times 10^8 \text{ m/s} \quad (2.15)$$

The impedance of the elemental transmission lines is

$$Z_{\text{elemental line}} = \sqrt{L/C} = Z_o = 377 \Omega \quad (2.16)$$

The medium modelled by the entire mesh of transmission lines is represented by the material properties $\mu = L, \epsilon = 2C$ (equation (2.11)). Therefore, the speed of propagation through the medium modelled by the mesh of transmission lines is

$$v_{mesh} = \frac{1}{\sqrt{\mu\epsilon}} = \frac{1}{\sqrt{2LC}} = \frac{c_0}{\sqrt{2}} \quad (2.17)$$

and the intrinsic impedance is

$$Z_{mesh} = \sqrt{\frac{\mu}{\epsilon}} = \sqrt{\frac{L}{2C}} = \frac{Z_0}{\sqrt{2}} \quad (2.18)$$

Usually the media properties of the elemental transmission lines are normalized. Hence the distributed inductance and capacitance of the transmission lines are ($L=1, C=1$). The velocity of propagation and the impedance of the elemental transmission lines are

$$v_{elemental\ line} = 1 \quad (2.19)$$

and

$$Z_{elemental\ line} = 1 \quad (2.20)$$

The media properties of the medium modelled by the mesh of transmission lines are therefore $\mu=1, \epsilon=2$. The resulting velocity of propagation, and intrinsic impedance are

$$v_{mesh} = \frac{1}{\sqrt{2}} \quad (2.21)$$

and

$$Z_{mesh} = \frac{1}{\sqrt{2}} \quad (2.22)$$

It is important to distinguish between the characteristics of the elemental transmission lines and the characteristics of the medium modelled by the mesh of elemental transmission lines.

2.1.3. Two Dimensional Series Node

The shunt node (Figure 2.4) can simulate either TE or TM propagation because of the dual nature of electric and magnetic fields. Another transmission line node can be derived to simulate either TE or TM propagation in two dimensions. The transmission line model is obtained from a lumped element model as in sections 1.1 and 1.2 of this chapter. The lumped element model in Figure 2.5(a) can be used as a building block from which an entire mesh can be constructed [19]. The mesh can be shown to satisfy an approximation to [15]

$$\frac{\partial i}{\partial x} = -C \frac{\partial v_y}{\partial t} \quad (2.23a)$$

$$\frac{\partial i}{\partial y} = C \frac{\partial v_x}{\partial t} \quad (2.23b)$$

$$\frac{\partial v_y}{\partial x} - \frac{\partial v_x}{\partial y} = 2L \frac{\partial i}{\partial t} \quad (2.23c)$$

Examining equations (2.23) and the set of Maxwell's equations for two dimensional TM propagation (2.3), the following set of relationships between field quantities in Maxwell's equations and circuit quantities in the lumped element network in Figure 2.5(a) can be established;

$$v_y = E_y$$

$$v_x = E_x$$

$$i = H_z$$

$$\mu = 2L, \text{ and } \epsilon = C \quad (2.24)$$

In addition, an equivalence between equations (2.23) and Maxwell's equations for two dimensional TE propagation (2.2) can be established. From the lumped element node in Figure 2.5(a), the transmission line node in Figure 2.5(b) can be constructed [19]. An entire mesh of transmission lines can be constructed to model either TE or TM

propagation using this node. The transmission lines in this model are connected in series and the transmission line node is referred to as the two dimensional TLM series node.

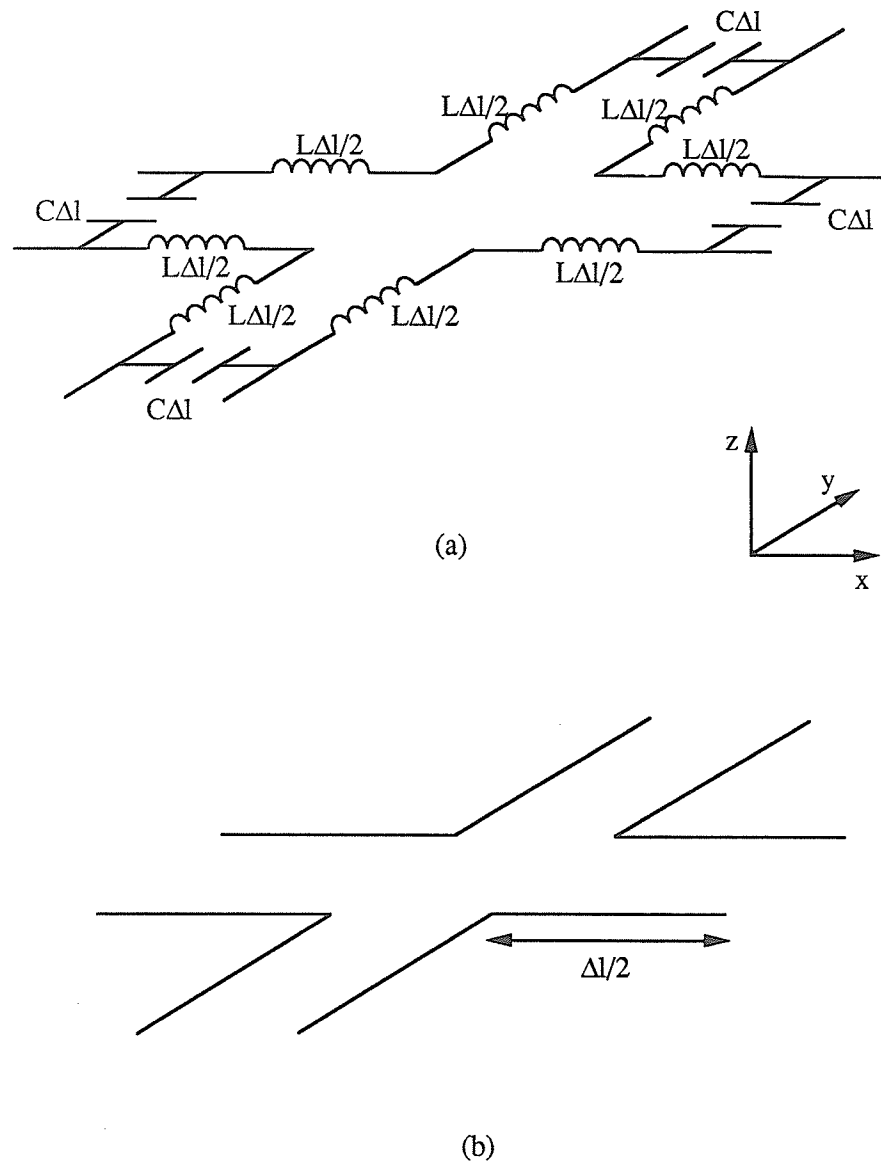


Figure 2.5: The two dimensional TLM series node represented as (a) lumped element network and (b) series intersection of transmission lines.

If the elemental transmission lines in Figure 2.5(b) are considered to represent a normalized free space, the medium modelled by the mesh is represented by

$$v_{mesh} = \frac{1}{\sqrt{2}} \quad (2.25)$$

and

$$Z_{mesh} = \sqrt{2} \quad (2.26)$$

The series node is of no value for problems with lossless homogeneous media because the shunt node can be used to model both sets of equations. For lossy inhomogeneous media, modifications to the shunt and series nodes are required. Under these modifications the shunt node is only valid for TE propagation, and the series node is only valid for TM propagation. The dual nature of electric and magnetic fields is no longer true, both models are only valid for the $V \equiv E$ and $I \equiv H$ analogy.

2.1.4. Representation of an Arbitrary Medium with a Transmission Line Model

In this section the modifications to the shunt node are presented. Maxwell's equations for a medium of permittivity ϵ , permeability μ , and conductivity σ are given as

$$\nabla \times \mathbf{H} = \epsilon \frac{\partial \mathbf{E}}{\partial t} + \sigma \mathbf{E} \quad (2.27a)$$

$$\nabla \times \mathbf{E} = -\mu \frac{\partial \mathbf{H}}{\partial t} \quad (2.27b)$$

Considering only two dimensional problems with no variation in the z direction, (2.27) yields two independent sets of equations. Equations (2.28) represent Maxwell's equations for two dimensional TE propagation

$$\frac{\partial E_z}{\partial x} = \mu \frac{\partial H_y}{\partial t} \quad (2.28a)$$

$$\frac{\partial E_z}{\partial y} = -\mu \frac{\partial H_x}{\partial t} \quad (2.28b)$$

$$\frac{\partial H_y}{\partial x} - \frac{\partial H_x}{\partial y} = \epsilon \frac{\partial E_z}{\partial t} + \sigma E_z \quad (2.28c)$$

and equations (2.29) represent Maxwell's equations for two dimensional TM propagation.

$$-\frac{\partial H_z}{\partial x} = \epsilon \frac{\partial E_y}{\partial t} + \sigma E_y \quad (2.29a)$$

$$\frac{\partial H_z}{\partial y} = \epsilon \frac{\partial E_x}{\partial t} + \sigma E_x \quad (2.29b)$$

$$\frac{\partial E_y}{\partial x} - \frac{\partial E_x}{\partial y} = -\mu \frac{\partial H_z}{\partial t} \quad (2.29c)$$

To simulate a medium of arbitrary permittivity, an open circuit transmission line stub of length $\Delta l/2$ and characteristic admittance Y_o is added to the shunt node [20]. A topological view of the shunt node loaded with an open circuit stub is shown in Figure 2.6(a). The effect of the open circuit line is to slow down the propagation of waves through the mesh. Part of the energy incident on the node is injected into the open circuit stub and then returned at the next time step. If the distributed inductance and capacitance of the open circuit line is selected to be

$$L_{o.c. stub} = \frac{L}{Y_o} \quad (2.30)$$

and

$$C_{o.c. stub} = CY_o \quad (2.31)$$

The speed of propagation along the line is then identical to that along the other elemental lines

$$v = \frac{1}{\sqrt{L_{o.c. stub} C_{o.c. stub}}} = \frac{1}{\sqrt{\frac{L}{Y_o} CY_o}} = \frac{1}{\sqrt{LC}} = \frac{\Delta l}{\Delta t} \quad (2.32)$$

The length of the stub is $\Delta l/2$ and therefore the energy is returned to the node after

one time step Δt . The amount of incident energy delayed by one time step is controlled by the admittance of the line, Y_o . The increase in permittivity due to the open circuit stub can be determined from the corresponding increase in capacitance that the stub adds to the network. The total capacitance of the node without the stub is $2C \Delta l$, and with the stub, $2C \Delta l + Y_o C \Delta l / 2$. The permittivity of the medium modelled by a mesh of stub loaded nodes is

$$\epsilon = 2 \left[1 + \frac{Y_o}{4} \right] \quad (2.33)$$

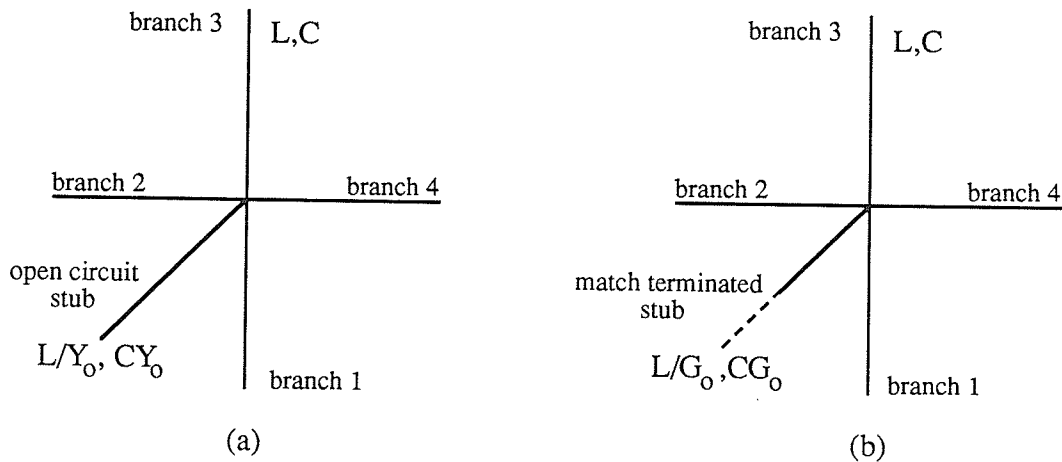


Figure 2.6: Modifications to the two dimensional TLM shunt node to model arbitrary media properties: (a) permittivity stub (b) loss stub.

The stub is terminated in an open circuit adding no inductance to the model. The propagation velocity and intrinsic impedance of the medium modelled by the mesh of transmission lines has been made variable by adding the stub, becoming

$$v_{mesh} = \frac{1}{\sqrt{2 \left[1 + \frac{Y_o}{4} \right]}} \quad (2.34)$$

and

$$Z_{mesh} = \frac{1}{\sqrt{2 \left[1 + \frac{Y_o}{4} \right]}} \quad (2.35)$$

To simulate a medium of arbitrary conductivity, a match terminated transmission line (or infinitely long transmission line) with a characteristic admittance of G_o is added as shown in Figure 2.6(b) [21]. The effect of the match terminated stub is to allow a portion of the energy incident upon the node to be absorbed at each time step. The amount of energy absorbed is controlled by the admittance of the line G_o . The distributed inductance and capacitance of the match terminated line is

$$L_{matched\ stub} = \frac{L}{G_o} \quad (2.36)$$

and

$$C_{matched\ stub} = CG_o \quad (2.37)$$

The conductivity of the medium is related to the characteristic admittance of the line by [21]

$$G_o = \sigma \Delta l \sqrt{\frac{\mu_o}{\epsilon_o}} \quad (2.38)$$

In TLM terminology, the open circuit line and match terminated lines are called permittivity and loss stubs respectively. For conductive mediums, the analogy between electric and magnetic fields no longer holds, because of the different form of equations (2.28) and (2.29). Therefore, the shunt node can only be used to simulate TE propagation and the series node can only be used to simulate TM propagation. The implementation of stubs for the series node is given in [21]. For a lossless medium, the shunt and series nodes are capable of modelling either TE or TM propagation. The permittivity stub of the shunt node would become a permeability stub, if TM propagation were considered.

2.1.5. Three Dimensional TLM

Consider the operation of shunt and series nodes in which the analogy ($E \equiv V, H \equiv I$) is always maintained. For an arbitrary two dimensional problem, a shunt node would be required to model TE propagation and a series node to model TM propagation. For an arbitrary three dimensional field problem, a shunt and series node would be required in each coordinate plane ($x-y, y-z, z-x$) to model all possible field distributions. In addition, the nodes in each coordinate plane must be interconnected to couple the fields in each plane. This interconnection of series and shunt nodes is the original three dimensional TLM node [22] and is referred to as an expanded node network. The elemental transmission lines of the shunt and series nodes are realized in two wire transmission lines (see Figure 2.7).

Although this node has been used extensively to model three dimensional field problems [23],[8],[24], there are problems associated with the use of the expanded node network. Consider a plane, parallel to one of the coordinate planes of the mesh. This plane intersects both series and shunt nodes due to the physical layout of the node (see Figure 2.7). To apply a boundary condition on the plane, voltage reflection coefficients are applied to the shunt nodes, and current reflection coefficients to the series nodes (as will be explained in section 3 of this chapter). For this reason, the application of boundary conditions is confusing and prone to error [25]. As well, problems with inhomogeneous material properties, dielectric and magnetic interfaces are separated from electric and magnetic walls by half a space step. This mis-alignment causes modelling errors in the analysis of microstrip and finline structures [7].

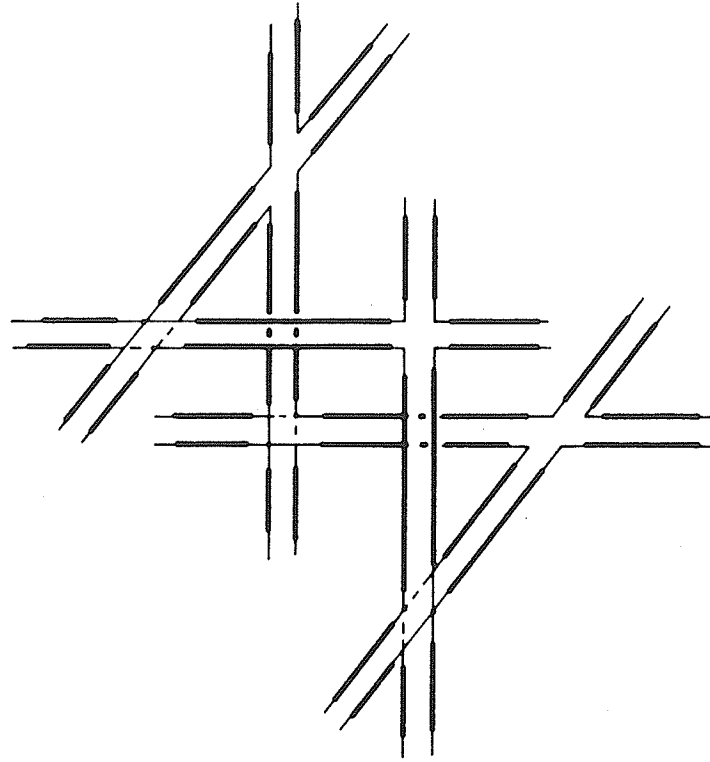


Figure 2.7: *Three dimensional expanded node consisting of an interconnection of series and shunt nodes realized in two wire transmission lines [22].*

To overcome the difficulties associated with the use of the expanded node, Johns has developed the symmetric condensed node [25] (see Figure 2.8). Again the elemental transmission lines making up the node, are two wire transmission lines. The node appears *symmetric* when viewed along each coordinate axis, thus eliminating the problems associated with applying boundary conditions. Field components are *condensed* to the centre of the node and all types of boundary conditions are applied at half space steps between nodes. This eliminates the misalignment difficulties of the expanded node. An additional benefit of using the symmetric condensed node is its superior propagation characteristics compared to the expanded node [26].

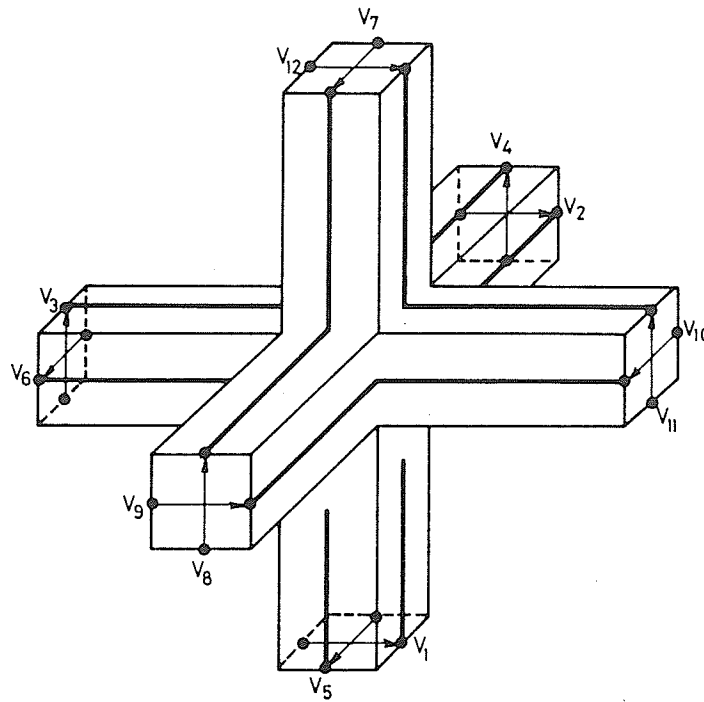


Figure 2.8: *Three dimensional symmetric condensed node [25].*

2.2. Computer Simulation of the Transmission Line Network

In the previous section a general method was shown to be capable of solving Maxwell's equations in the time domain. To provide a solution to a specific problem, boundary conditions and initial conditions are required. The details of solving the transmission line network by computer simulation are provided in this section.

2.2.1. Algorithm

The TLM algorithm operates by scattering impulses off the transmission line junctions and then transferring the impulses from one node to the next. Since the elemental transmission line elements are considered to be ideal, the impulses propagate without dispersion or distortion. As well, the scattering event is characterized by examining the impedance discontinuity encountered by an impulse approaching a junction. For these reasons, an exact solution to the impulse response of the transmission line network can be obtained.

In general, the TLM algorithm can be classified as comprising of a scattering event \mathbf{S} relating incident impulses to reflected impulses at each time step at each node,

$$\mathbf{V}^r = \mathbf{S} \mathbf{V}^i \quad (2.39)$$

and then transferring the reflected impulse to become incident impulses on adjacent transmission lines, at the next time step. The transferring is accomplished by a connection matrix \mathbf{C} ,

$$\mathbf{V}^i = \mathbf{C} \mathbf{V}^r \quad (2.40)$$

where \mathbf{V}^i and \mathbf{V}^r are vectors containing incident and reflected voltages respectively, at each node. This formulation of the TLM method has been used by Johns [27] and Johns and Butler [28] to perform some theoretical investigations of the method. In a practical situation a TLM computer program does not operate exactly as (2.39) and (2.40). At each node, (2.39) is performed where \mathbf{S} would represent the scattering matrix of a single node, and the vectors $\mathbf{V}^i, \mathbf{V}^r$ are the incident and reflected impulses at the node. The scattering matrix of a shunt node without permittivity or loss stubs can be obtained by examining the transmission and reflection coefficients seen by an impulse incident on the transmission line junction. Consider the shunt node in Figure 2.9(a) with a unit magnitude voltage impulse v_1 incident on line 1. In a normalized

transmission line mesh, the impedance of each elemental line is 1. Looking into the junction, the impulse will see three lines of unit impedance connected in parallel, or a load impedance of $1/3$. The voltage reflection coefficient seen by the impulse is

$$\Gamma = \frac{Z_L - Z_o}{Z_L + Z_o} = -\frac{1}{2} \quad (2.41)$$

The transmission coefficient seen by the impulse is

$$T = \frac{Z_o - Z_L}{Z_o + Z_L} = \frac{1}{2} \quad (2.42)$$

After the scattering event takes place, the reflected impulses due to the incident impulse $v_1^i = 1, v_2^i = 0, v_3^i = 0, v_4^i = 0$ are $v_1^r = -1/2, v_2^r = 1/2, v_3^r = 1/2, v_4^r = 1/2$ (see Figure 2.9(b)). Due to the symmetry of the node, the same type of behavior is observed for a unit impulse incident on any branch with no other excitation.

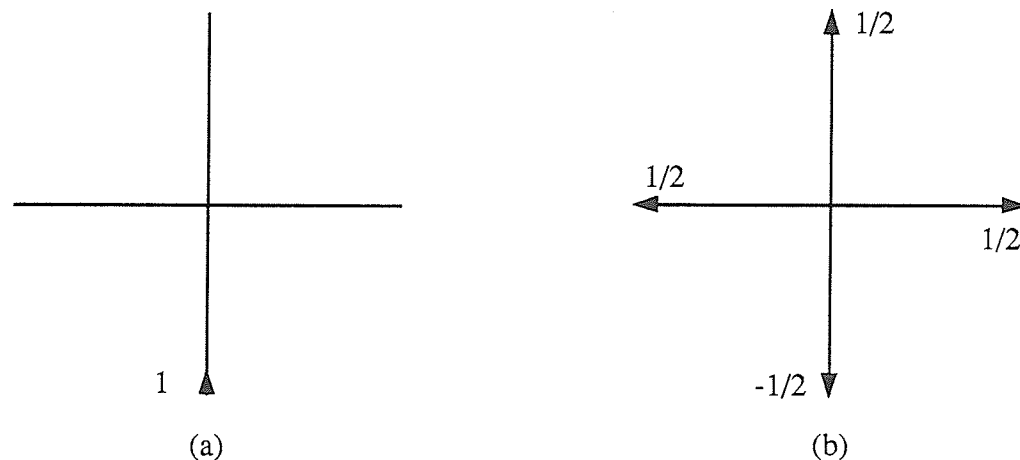


Figure 2.9: Scattering of a unit magnitude impulse incident on branch 1 of a shunt node without stubs, (a) before scattering event (b) after scattering event.

The property of superposition can be applied to determine the behavior of the mesh with more than one non zero incident pulse. The voltage scattering matrix of a shunt

node without stubs is

$$\begin{bmatrix} v_1^r \\ v_2^r \\ v_3^r \\ v_4^r \end{bmatrix} = \frac{1}{2} \begin{bmatrix} -1 & 1 & 1 & 1 \\ 1 & -1 & 1 & 1 \\ 1 & 1 & -1 & 1 \\ 1 & 1 & 1 & -1 \end{bmatrix} \begin{bmatrix} v_1^i \\ v_2^i \\ v_3^i \\ v_4^i \end{bmatrix} \quad (2.43)$$

In a TLM computer program the scattering event is implemented as

$$v_n^r = \frac{1}{2} \left(\sum_{j=1}^4 v_j^i \right) - v_n^i \quad (2.44)$$

The reflected impulses are transferred to adjacent nodes using [6]

$$v_1^i(x, y) = v_3^r(x, y - \Delta l) \quad (2.45a)$$

$$v_2^i(x, y) = v_4^r(x - \Delta l, y) \quad (2.45b)$$

$$v_3^i(x, y) = v_1^r(x, y + \Delta l) \quad (2.45c)$$

$$v_4^i(x, y) = v_2^r(x + \Delta l, y) \quad (2.45d)$$

The propagation of an impulsive disturbance through a mesh of shunt nodes is shown in Figure 2.10 [29].

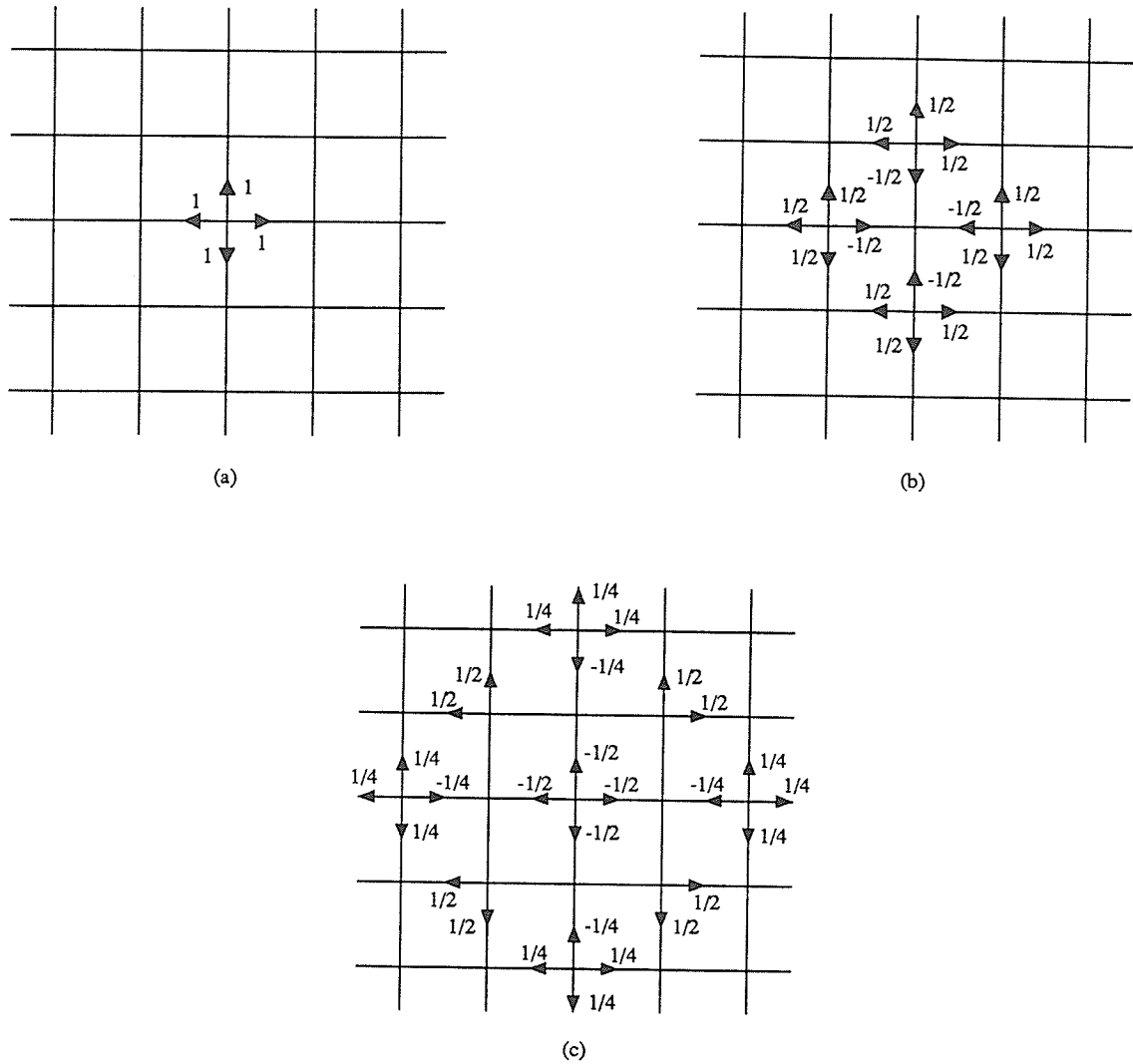


Figure 2.10: Propagation of an impulsive disturbance through a mesh of shunt nodes.

The scattering matrix for the shunt node loaded with permittivity and loss stubs is derived by examining the reflection and transmission coefficients on each line. The effect of the loss stub is only to extract energy from the node. The voltage impulse transmitted into the stub is not stored, although the effect of the stub is included. The scattering matrix for the stub loaded shunt node as derived by Akhtarzad and Johns

[21] is

$$\mathbf{S} = \frac{2}{Y} \begin{bmatrix} 1 & 1 & 1 & 1 & Y_o \\ 1 & 1 & 1 & 1 & Y_o \\ 1 & 1 & 1 & 1 & Y_o \\ 1 & 1 & 1 & 1 & Y_o \\ 1 & 1 & 1 & 1 & Y_o \end{bmatrix} - \mathbf{I} \quad (2.46)$$

where $Y = 4 + Y_o + G_o$ and \mathbf{I} is the unit matrix.

For the case $G_o = 0$, the scattering matrix is unitary (i.e., $\mathbf{S}\mathbf{S}^* = \mathbf{I}$) [30] indicating a lossless junction. Obviously with the inclusion of the loss stub, it will no longer be unitary.

2.2.2. Boundary Conditions

Boundary conditions are enforced by terminating the elemental transmission lines using reflection coefficients specified at points half way between nodes, or at the centre of nodes. This requirement is to ensure synchronism of impulses at nodal points.

To apply the proper reflection coefficient, the type of mesh used (series or shunt) and the relationship between field quantities and circuit quantities must be established ($V \equiv E, I \equiv H$ or $V \equiv H, I \equiv E$). A transmission line matrix consisting of shunt nodes simulates a wave equation of the voltage in the mesh. Therefore, voltage reflection coefficients are used to specify boundary conditions. The voltage reflection coefficient Γ_v for load impedance Z_L in a medium with intrinsic impedance Z_o is

$$\Gamma_v = \frac{Z_L - Z_o}{Z_L + Z_o} \quad (2.47)$$

Similarly, a transmission line matrix consisting of series nodes simulates the wave equation of the current in the mesh. Therefore, current reflection coefficients are used to specify boundary conditions. The current reflection coefficient associated with a load

impedance Z_L in a medium of characteristic impedance Z_o is

$$\Gamma_c = \frac{Z_o - Z_L}{Z_o + Z_L} \quad (2.48)$$

In the above discussion, the impedances refer to the impedances as defined for the circuit quantities in the model and not the field quantities they represent. As noted in section 1.2 of this chapter, the TLM shunt and series nodes are capable of representing both TE and TM propagation. If a mesh of shunt nodes is used to simulate TE propagation, the $V \equiv E, I \equiv H$ analogy is used. For these cases, the circuit impedance values $Z_C = V/I$ correspond to the field impedance value $Z_F = E/H$ and therefore, either Z_C or Z_F should be used in the expressions for the reflection coefficients. However, if the $V \equiv H, I \equiv E$ analogy is used, the circuit impedance value $Z_C = V/I$ corresponds to the field admittance value $Y_F = H/E$ and therefore Y_F should be used as the impedance value Z_L in the expressions for the reflection coefficients.

Boundary conditions frequently found in TLM simulations are: perfect conductors, magnetic walls, material interfaces, and free space boundaries. Perfect conductors are represented by reflection coefficients corresponding to $Z_F = 0$. Magnetic walls are used to reduce the size of a problem without altering the results of the simulation. In waveguide problems, symmetry can be exploited to reduce the size of the simulation space. Special treatment of material interfaces are sometimes required [20]. These boundaries are realized by using reflection and transmission coefficients between nodes on either side of the boundary. In the past, free space boundaries have been realized by match terminating the TLM mesh. To match terminate a TLM mesh, the elemental transmission lines are terminated in the intrinsic impedance of the medium modelled by the mesh. A shunt mesh loaded with permittivity stubs represents a medium with permittivity

$$\epsilon = 2 \left[1 + \frac{Y_o}{4} \right] \quad (2.49)$$

permeability

$$\mu = 1 \quad (2.50)$$

and therefore an intrinsic impedance of

$$Z_o = \frac{1}{\sqrt{2} \left[1 + \frac{Y_o}{4} \right]} \quad (2.51)$$

The reflection coefficient required to achieve match termination of the mesh is

$$\Gamma = \frac{\frac{1}{\sqrt{2} \left[1 + \frac{Y_o}{4} \right]} - 1}{\frac{1}{\sqrt{2} \left[1 + \frac{Y_o}{4} \right]} + 1} \quad (2.52)$$

Again, the difference between the elemental transmission lines and the medium they represent is obvious. The reflection coefficient (2.52) does not match terminate the elemental transmission lines (a reflection coefficient $\Gamma=0$ would be required) but it provides a match termination of the medium modelled by the mesh of elemental transmission lines. In practice, terminating the elemental transmission lines in (2.52) provides accurate absorption of waves with normal incidence to the boundary. Waves incident at arbitrary angles are not accurately absorbed. Chapter 5 discusses the general topic of absorbing boundary conditions.

One of the limitations of the TLM method compared to finite element or boundary element techniques is the requirement of enforcing boundary conditions at locations half way between nodes. An example of fitting a rectangular grid to a smoothly

curved boundary is shown in Figure 2.11. Finite element and boundary element methods use isoparametric elements to accurately model curved surfaces.

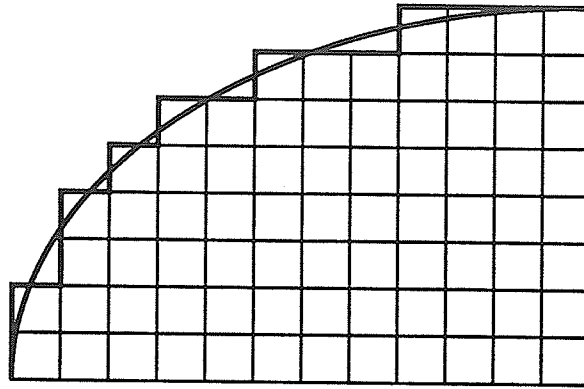


Figure 2.11: *Modelling of a curved boundary with a rectangular TLM mesh.*

In practice, the errors caused by the approximation of curved boundaries with a piece wise straight boundary are only noticeable at high frequencies. At low frequencies the wavelength is large enough so that the inaccuracies in the boundaries are not resolved. However, at high frequencies the poorly modelled boundary is resolved by the small wavelength thus producing errors.

Johns and Butler [31] developed a scheme that models curved boundaries. The scattering events at nodes neighboring the boundaries are reformulated to account for elemental transmission lines of arbitrary length. Unfortunately, the approximations used in the reformulation of the scattering event are only valid at low frequencies, therefore not correcting the problem noted above.

2.2.3. Obtaining Frequency Domain Results from a Time Domain Simulation

To obtain the time domain response of a structure, an output point is specified. At each time step, the desired field quantity is computed from circuit quantities on the elemental lines. To obtain the frequency response, an impulsive excitation is used and the desired field quantity is computed and stored at each iteration step. The real and imaginary parts of the frequency response $F(\Delta l/\lambda)$ are calculated by Fourier transforming the impulse response:

$$\text{Re} \left\{ F(\Delta l/\lambda) \right\} = \sum_{n=1}^N I_n \cos(2\pi n \frac{\Delta l}{\lambda})$$

$$\text{Im} \left\{ F(\Delta l/\lambda) \right\} = \sum_{n=1}^N I_n \sin(2\pi n \frac{\Delta l}{\lambda})$$

where I_n is the value of the impulse response at the n^{th} time step N is the total number of iterations. Thus the entire frequency response is obtained from the single TLM simulation of the model.

2.3. Errors in TLM Simulations and their Correction

In general, three types of errors are present in a TLM simulation.

- 1) truncation error - due to the finite duration of the impulse response
- 2) velocity error - the dependence of the velocity of propagation through the mesh on the wavelength (and direction of propagation)
- 3) coarseness error - the inability of the TLM mesh to resolve highly non uniform field distributions

The three groups of errors have been summarized by Hofer in his review paper [7]. Each error is discussed along with methods for minimization.

2.3.1. Truncation Error

Truncation error occurs only if time domain results are Fourier transformed into the frequency domain. This error does not occur if only time domain data is required. The truncation error occurs because the iteration process must be stopped at a finite point in time. Two methods are used to minimize truncation error. The first method is to increase the number of iterations at the expense of cpu time. The second is to use a filter while performing the Fourier transformation. Saguet and Pic have demonstrated that a Hanning window provides increased accuracy of frequency domain results and a corresponding decrease in the number of iterations required to provide convergent results [32].

2.3.2. Velocity Error

Velocity error is due to the dependence of the velocity of waves through the mesh on both frequency and direction of propagation. The mesh can be considered as a periodic structure for diagonal and axial propagation. Expressions for the ratio of phase velocity of waves travelling through the mesh, to the velocity of impulses on the elemental lines can be determined from analysis of the periodic structure. The velocity error is not significant at low frequencies $\Delta l/\lambda \leq 0.1$, because the propagation characteristics of the mesh are independent of frequency and direction. Therefore the electrical size of the problem modelled and frequency range of interest should be considered during the layout of the TLM simulation space. Dispersive errors in TLM simulations and time domain methods in general are discussed in Chapter 3.

2.3.3. Coarseness Error

Coarseness error results from the inability of the TLM method to resolve rapid variations in the field distributions. To reduce this error, a fine mesh can be used to increase the accuracy of the simulation. However, the use of a fine mesh throughout the entire problem is unnecessary and results in excessive computational costs. A variable mesh scheme was developed independently by Saguet and Pic [33] and Al-Mukhtar and Sitch [34],[35]. The variable mesh allows fine discretization in regions containing rapid field variation and a coarse discretization in regions of slowly varying fields.

All three errors are present in any TLM simulation and steps should be taken to minimize them. Truncation error is present in all time domain methods in which impulsive excitation and Fourier transformation are used to obtain frequency domain results. Coarseness error is present in all numerical methods and is a result of the discrete nature of computational models. The accuracy of the TLM propagation model is characterized by the velocity error, or the dispersion characteristic of the method (discussed in Chapter 3).

2.4. Applications of the TLM Method

The TLM method has been successfully applied to the analysis of transmission line structures. A comprehensive list of the applications can be found in Hoefler's review paper [7]. Most of the applications deal with the analysis of microwave circuits. The TLM method has also been used to perform transient analysis of non-linear circuits [36],[37] and to solve diffusion problems [27],[28]. This thesis covers the application of the TLM method to electromagnetic scattering problems. Problems of this nature have not received much attention. The following section provides a review

of the previous attempts at applying the TLM method to open region problems and examines the boundary conditions used to terminate the simulation space.

2.4.1. TLM and Open Region Problems

Pompei *et al* used the TLM method to examine the group and phase velocity on microstrip lines [38],[8] and to characterize dipole and microstrip antennas [39]. Two methods were used to model an infinite simulation space. The first method described utilizes a sufficiently large mesh so that the iteration process is terminated before the waves reflected by the imperfect exterior boundaries return to the observation points. Although this method accurately simulates an infinite mesh, cpu time and storage requirements are excessive for complicated problems. The second method used is to terminate the elemental transmission lines of the model in the intrinsic impedance of the medium modelled by the mesh (discussed previously). Accurate results are presented for group and phase velocities on microstrip lines. The impedance and resonant frequency calculations for the microstrip antennas differed from experimental and moment method calculations by a few percent [39]. An improved mesh termination condition would increase the accuracy of the results.

Ney and Yue applied the TLM method to two dimensional scattering by a dielectric cylinder [40]. To match terminate the TLM mesh, they also terminated the elemental lines in the impedance of the medium modelled by the mesh. Sinusoidal excitation rather than a pulse was used and results for the scattered field at a single frequency were presented. Significant errors were present in the results. Ney and Yue suggest two reasons for the poor results. The first reason is the iteration process was terminated before a steady state condition was reached. The second is that the boundary condition used to terminate the mesh was inaccurate. A significant point made by Ney and Yue not previously mentioned in the literature, was that termination in the

impedance of the medium modelled by the mesh, does not provide a reflectionless termination of the simulation space. This point will be discussed in Chapter 4.

Ney and Yue made two suggestions to improve the termination condition. The first suggestion was to modify the impedance values used to terminate the mesh until no standing waves are observed. This type of scheme would be very inefficient as several simulations would be required before the impedance values were adjusted to obtain suitable accuracy. In addition, re-adjustment of impedance values would be required for each new frequency selected or scattering object. The second suggestion made by Ney and Yue was to use artificial walls consisting of nodes loaded with permittivity and conductivity stubs, to gradually absorb the outgoing waves. This type of scheme was investigated by Taflove and Brodwin in the early development of FDTD methods for scattering applications [41]. At the mesh boundary, Taflove and Brodwin suggest using linearly increasing values of conductivity to gradually absorb the outgoing radiation. The distance required to absorb the waves was found to be of the order of one wavelength. This is an unacceptably large distance for use with FDTD and TLM algorithms as excessive cpu time and memory storage would be required for such distances. Recently, these types of absorbing boundary conditions have received attention among FDTD researchers. Taflove and Umashankar [42], and Taflove and Strickel [43] have investigated the use of electric and magnetic losses to absorb outgoing waves. A wave absorber placed around the exterior of the mesh is synthesized in non physical layers of varying permittivity, permeability, and electric and magnetic conductivities adjusted using non linear optimization. In addition, Yoshida and Fukai [44] have used absorbing materials along the outside edges of the mesh as absorbing boundary conditions. This type of termination is not suitable in this investigation because it is only effective over a narrow bandwidth.

German *et al* used the TLM method to perform full wave analysis of passive microstrip components [45] and microstrip antennas [46]. They state "... *very highly absorbing continuation boundaries*" [46] and "... *perfectly absorbing boundary conditions*" [45] have been developed, however, references or details regarding the boundary conditions are not included. In addition, the authors state "... *reflectionless truncation of the problem space is straightforward*" [46] and the conditions developed are for use with graded and anisotropic meshes. The work performed by Ney and Yue [40], by Pompei *et al* [38], and the results presented in Chapter 6 indicate that reflectionless termination of the problem space is not straightforward. It is likely that German *et al* have used the traditional match termination procedure and have extended this to graded and anisotropic meshes. Such conditions are less than perfectly absorbing, indicating that the results reported could be improved upon.

Johns *et al* have applied the TLM method to examine three dimensional scattering problems [26]. The purpose of the paper [26] was to apply the three dimensional symmetric condensed node (introduced in a companion paper [25]) to various electromagnetic field problems. The electromagnetic pulse (EMP) response of an F-111 aircraft was examined. Time domain results for the axial current density on the top face of the fuselage are given. Results reported agree with measurements and finite difference simulations. Again, termination of the elemental lines in the impedance of the medium modelled by the elemental transmission lines is used to terminate the TLM space.

The research reviewed represents initial investigations of the TLM method to the solution of unbounded field problems. All of the researchers indicate the TLM method is a simple yet powerful tool for the analysis of electromagnetic field problems. The accuracy and efficiency of TLM simulations of open region field problems can be increased by improving the absorbing boundary conditions used to model an infinite space.

Chapter 3

Comparison of TLM and Similar Methods

The TLM method simulates electromagnetic fields in both space and time. In this chapter, TLM is compared with two other methods also capable of simulating electromagnetic fields in space and time, the Finite Difference-Time Domain method (FD-TD) and Beregeron's method. The FD-TD method as developed by Yee [2] is based on difference approximations of Maxwell's equations. The method has been successfully applied to a variety of problems as summarized by Taflove [47]. Some previous comparisons of the TLM and FD-TD methods have been made in the past [48]. The relationship in two dimensions is thoroughly investigated in this chapter. Beregeron's method or the Spatial Network Method (SNM), as developed by Yoshida and Fukai [17],[44] is theoretically similar to the TLM method, as it is based on the equivalent circuit of Maxwell's equations. Its relationship with the TLM method and the accuracy of lumped element models of Maxwell's equations is discussed.

The FD-TD method has been extensively and successfully applied to open region problems while the TLM method has only recently been applied to such problems. Establishing relationships between similar numerical methods will allow developments made in one method to be more easily applied to the other, helping researchers using either method.

3.1. Comparison of TLM and FD-TD

In this section the relationship between the TLM and FD-TD methods is examined. A review of previous comparisons of TLM and FD-TD methods is provided along with a brief review of the FD-TD method in two dimensions. The relationship between the two methods is established in two ways. First, by showing that the TLM method can be operated in such a way that it satisfies the FD-TD equations in two dimensions (as stated by Johns for three dimensional simulations [48]). Second, by deriving dispersion relations for the methods in a medium with arbitrary permittivity and conductivity and determining the conditions for which the dispersion relations are identical. Both comparisons explicitly show the relationship between the two methods.

3.1.1. Previous Comparisons of TLM and FD-TD

Previous comparisons of TLM and finite difference methods in electromagnetics [48] and in diffusion problems [27],[28] have involved the complete solution of a problem including boundary conditions. In this chapter the emphasis is placed on wave propagation mechanisms by examining individual nodes.

In previous comparisons the formulation of the TLM method is expressed as,

$${}_k \mathbf{V}^r = \mathbf{S} {}_k \mathbf{V}^i \quad (3.1)$$

and

$${}_{k+1} \mathbf{V}^i = \mathbf{C} {}_k \mathbf{V}^r \quad (3.2)$$

where ${}_k \mathbf{V}^i$ and ${}_k \mathbf{V}^r$ are the vectors of the incident and reflected voltages at all nodes at time step k , \mathbf{S} is the scattering event involving all nodes in the mesh, and \mathbf{C} is the connection matrix describing how nodes are connected to each other (including boundary conditions). These two equations include all information required to solve the transmission line model, including boundary conditions.

Johns has shown mathematically that for TLM and finite difference simulations to be equivalent, the connection matrix \mathbf{C} must satisfy $\mathbf{C}\mathbf{C}=\mathbf{I}$ [27]. This means physically that boundary conditions in the TLM model are expressed in terms of field quantities only as is the case in finite difference algorithms. This is not the usual way of specifying boundary conditions in a TLM simulation. In TLM simulations boundaries are located half way between nodal locations and operate by means of reflection coefficients (as discussed in Chapter 2). However, for an arbitrary boundary termination, the TLM description consisting of reflection and transmission coefficients can not be expressed in terms of the field quantities alone, and therefore does not correspond to a condition that can be incorporated into FD-TD simulations. Although the two methods are shown to propagate waves in the same manner, the entire simulation is not identical because of the unique specification of boundary conditions for each method.

3.1.2. Comparison of Time Stepping Procedures

The previous comparisons of the TLM and FD-TD methods have required the formulation of the TLM method in terms of global scattering and connection matrices. In this section, the relationship is established by examining the scattering and transferring of individual impulses on small groups of nodes over a few iteration steps. Although the comparison techniques are simplistic, they allow better visualization of how the scattering of impulses off transmission line junctions and transferral to adjacent nodes satisfies the FD-TD equations. Comparison of the methods through examination of individual nodes is considered to be important because most developments are implemented at the level of individual nodes. Establishing relationships at the level of individual nodes will help the transfer of developments between methods.

3.1.2.1. Review of the FD-TD Method

An extensive review of the TLM method was presented in the previous chapter. The following is a brief description of the FD-TD method. A detailed discussion of the algorithm can be found in [2] and [41]. Sufficient detail is provided to allow familiarity with the method.

The original paper describing the FD-TD method was written by Yee in 1966 [2]. A concise description of the FD-TD algorithm used to model two dimensional electromagnetic fields for transverse electric (TE) propagation can be found in a recent paper by Blaschak and Kriegsmann [49]. Maxwell's equations for two dimensional TE propagation independent of the z direction are,

$$\frac{\partial E_z}{\partial y} = -\mu \frac{\partial H_x}{\partial t} \quad (3.3a)$$

$$\frac{\partial E_z}{\partial x} = \mu \frac{\partial H_y}{\partial t} \quad (3.3b)$$

$$\frac{\partial H_y}{\partial x} - \frac{\partial H_x}{\partial y} = \sigma E_z + \epsilon \frac{\partial E_z}{\partial t} \quad (3.3c)$$

The FD-TD algorithm discretizes equations (3.3) in both space and time using the following central difference expression,

$$\frac{\partial f}{\partial \eta} = \frac{f \left[\eta + \frac{\Delta \eta}{2} \right] - f \left[\eta - \frac{\Delta \eta}{2} \right]}{\Delta \eta} \quad \mathbf{O}(\Delta \eta)^2 \quad (3.4)$$

In order to apply the difference expression to equations (3.3) the electric and magnetic field components are placed at half space increments from each other and evaluated at alternate time steps [2]. The physical layout of the positions at which field components are defined are shown in Figure 3.1 [49].

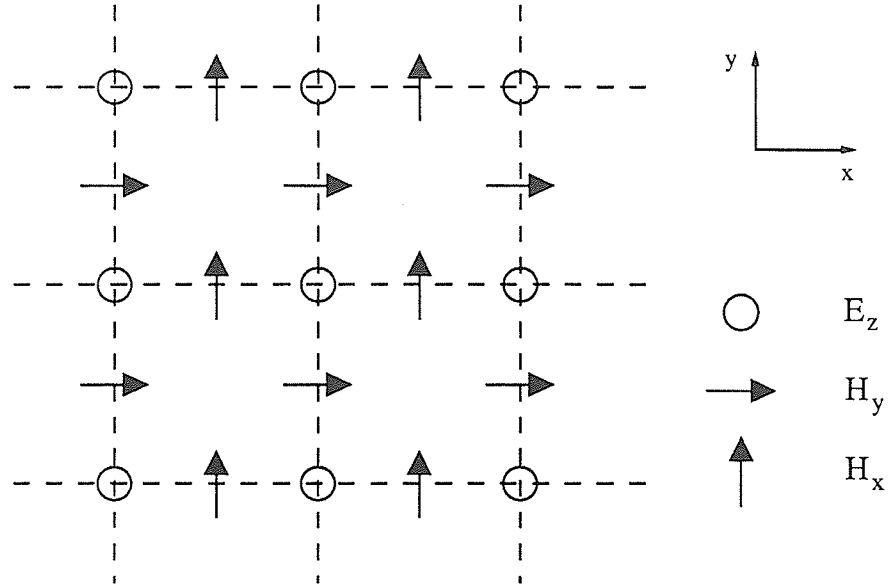


Figure 3.1: Physical layout of field quantities on a two dimensional FD-TD grid [49].

Considering a non conductive medium ($\sigma=0$) equation (3.4) can be used to discretize equations (3.3),

$$\frac{E_z^{t+\frac{\Delta t}{2}}(x,y+\Delta l) - E_z^{t+\frac{\Delta t}{2}}(x,y)}{\Delta y} = -\mu \frac{H_x^{t+\Delta t}(x,y+\frac{\Delta l}{2}) - H_x^t(x,y+\frac{\Delta l}{2})}{\Delta t} \quad (3.5a)$$

$$\frac{E_z^{t+\frac{\Delta t}{2}}(x+\Delta l,y) - E_z^{t+\frac{\Delta t}{2}}(x,y)}{\Delta x} = \mu \frac{H_y^{t+\Delta t}(x+\frac{\Delta l}{2},y) - H_y^t(x+\frac{\Delta l}{2},y)}{\Delta t} \quad (3.5b)$$

$$\begin{aligned} \frac{H_y^t(x+\frac{\Delta l}{2},y) - H_y^t(x-\frac{\Delta l}{2},y)}{\Delta x} - \frac{H_x^t(x,y+\frac{\Delta l}{2}) - H_x^t(x,y-\frac{\Delta l}{2})}{\Delta y} \\ = \epsilon \frac{E_z^{t+\frac{\Delta t}{2}}(x,y) - E_z^{t-\frac{\Delta t}{2}}(x,y)}{\Delta t} \end{aligned} \quad (3.5c)$$

The space steps in the x and y directions are chosen to be equal ($\Delta x = \Delta y = \Delta l$), and the time step Δt must be chosen to satisfy the Courant stability limit [41],

$$\frac{\Delta t}{\Delta l} \leq \frac{1}{\sqrt{2}c} \quad (3.6)$$

Equations (3.5) can be re-arranged in order to obtain

$$H_x^{t+\Delta t}(x,y+\frac{\Delta l}{2}) = H_x^t(x,y+\frac{\Delta l}{2}) - \frac{\Delta t}{\mu\Delta l} \left[E_z^{t+\frac{\Delta t}{2}}(x,y+\Delta l) - E_z^{t+\frac{\Delta t}{2}}(x,y) \right] \quad (3.7a)$$

$$H_y^{t+\Delta t}(x+\frac{\Delta l}{2},y) = H_y^t(x+\frac{\Delta l}{2},y) + \frac{\Delta t}{\mu\Delta l} \left[E_z^{t+\frac{\Delta t}{2}}(x+\Delta l,y) - E_z^{t+\frac{\Delta t}{2}}(x,y) \right] \quad (3.7b)$$

$$\begin{aligned} E_z^{t+\frac{\Delta t}{2}}(x,y) = E_z^{t-\frac{\Delta t}{2}}(x,y) + \\ \frac{\Delta t}{\epsilon\Delta l} \left[H_y^t(x+\frac{\Delta l}{2},y) - H_y^t(x-\frac{\Delta l}{2},y) + H_x^t(x,y-\frac{\Delta l}{2}) - H_x^t(x,y+\frac{\Delta l}{2}) \right] \end{aligned} \quad (3.7c)$$

Expressions (3.7) relate the field quantities at a particular time step to field quantities at previous time steps. This enables the creation of a simple algorithm to iteratively calculate the field distribution in space as time progresses.

This scheme and its extension to three dimensions has generically become known in the electrical engineering literature as the Finite Difference Time Domain (FD-TD) method. Mathematically it is a finite difference algorithm using difference approximations of second order accuracy and a leap frog time stepping procedure [50].

3.1.2.2. Modified TLM Scheme

The two dimensional TLM shunt node developed by Johns and Akhtarzad [21] to model equations (3.3) is discussed in Chapter 2. The open circuit stub of characteristic admittance Y_o , and match terminated stub of characteristic admittance G_o , are used to model the permittivity and conductivity of the medium respectively. The media properties of the medium modelled by a mesh of these nodes are,

$$\epsilon_r = 2 \left[1 + \frac{Y_o}{4} \right] \quad (3.8)$$

$$\sigma = \frac{G_o}{\Delta l} \sqrt{\frac{\epsilon_o}{\mu_o}} \quad (3.9)$$

Consider a TLM mesh conforming to a discretized coordinate system $(i\Delta l, j\Delta l)$ in the $x-y$ plane, where i and j represent discretized coordinates in the x and y directions respectively. Each iteration step corresponds to a progression in time of Δt . In the original formulation of the TLM method [6] the field quantities are defined in time, when pulses are incident on the node ($t = n\Delta t$) and in space at the centre of nodes $(i\Delta l, j\Delta l)$. The field quantities are defined in terms of the circuit quantities as,

$$E_z = V_z \quad (3.10a)$$

$$H_x = -I_y \quad (3.10b)$$

$$H_y = I_x \quad (3.10c)$$

and in terms of the incident pulses on the transmission line model as,

$$E_z = \frac{1}{2}(v_1^i + v_2^i + v_3^i + v_4^i) \quad (3.11a)$$

$$H_x = v_3^i - v_1^i \quad (3.11b)$$

$$H_y = v_2^i - v_4^i \quad (3.11c)$$

where $v_1^i, v_2^i, v_3^i, v_4^i$ are incident pulses at a node at a particular iteration step [6].

In the original TLM formulation, electric and magnetic field quantities are defined at the same point in time and at the same point in space. Consider the following changes to the definitions of field quantities.

- 1) The electric field (E_z) is defined in space at the centre of the nodes $x=i\Delta l, y=j\Delta l$, but half a time step after pulses appear on the branches of the node $t=(n+1/2)\Delta t$, or in other words an infinitesimally small time step prior to the scattering event.
- 2) The magnetic fields (H_x, H_y) are defined in time when pulses first appear on the branches of a node ($n\Delta t$), and in space at positions where adjacent vertical and horizontal nodes join (H_x defined at $x=(i+1/2)\Delta l, y=j\Delta l$; H_y defined at $x=i\Delta l, y=(j+1/2)\Delta l$).

The relationships of the field quantities and circuit quantities (3.10) remain. These changes do not affect the operation of the node, but only the manner in which field quantities are defined in terms of the voltage impulses. Note that the new definitions for field quantities correspond in space and time to those used in FD-TD simulations shown in Figure 3.1.

The group of five nodes in Figure 3.2 can be used to illustrate the modified scheme. Consider this group of nodes as part of a larger mesh. The nodes are numbered from 1 to 5 as shown and branch numbers correspond to the orientation given in Figure 2.6. The permittivity and loss stubs have been omitted for simplicity. To distinguish distinct pulses on different nodes, the following terminology is used. A pulse defined as $v_{n,m}^t$ refers to the pulse incident on branch m of node n at time t . If a pulse is not an incident pulse (i.e., a reflected pulse) it is stated so explicitly.

At time step t pulses first appear on the branches of the nodes (see Figure 3.2(a)). The electric field is not defined at this time step. The magnetic fields H_x and H_y are defined at this time step and spatially at locations A,B; and C,D respectively as,

$$H_x^t(A) = -I_y(A) = -(v_{1,1}^t - v_{5,3}^t) \quad (3.12a)$$

$$H_x^t(C) = -I_y(C) = -(v_{3,1}^t - v_{1,3}^t) \quad (3.12b)$$

$$H_y^t(B) = I_x(B) = (v_{1,2}^t - v_{2,4}^t) \quad (3.12c)$$

$$H_y^t(D) = I_x(D) = (v_{4,2}^t - v_{1,4}^t) \quad (3.12d)$$

Note that magnetic fields are defined using impulses on adjacent nodes. In the original scheme, fields are always defined using pulses on the same node.

At time step $t = t_o + \Delta t/2$ (just before the scattering event takes place) pulses have reached the centre of the nodes (see Figure 3.2(b)). The electric fields are defined at this point in time using (3.11a). The electric field at nodal location 1 is,

$$E_z^{t+\frac{\Delta t}{2}}(\text{node } 1) = V_z(\text{node } 1) = \frac{1}{2}(v_{1,1}^t + v_{1,2}^t + v_{1,3}^t + v_{1,4}^t) \quad (3.12)$$

The definition of E_z at nodes 2, 3, 4, and 5 is defined in the same manner. After the scattering event takes place, the scattered pulses travel away from the centre of the nodes and at time $t + \Delta t$, new pulses $v_{n,m}^{t+\Delta t}$ are incident on the nodes. The new pulses are the reflected pulses from adjacent nodes at the previous time step. The magnetic field quantities H_x and H_y are again defined at locations A,C and B,D respectively using (3.12).

The modifications to the TLM scheme are not to suggest a new way of operating the mesh in practice. The modifications are used to show how the TLM algorithm can be operated in such a way that it will satisfy the difference approximations (3.7) to Maxwell's equations.

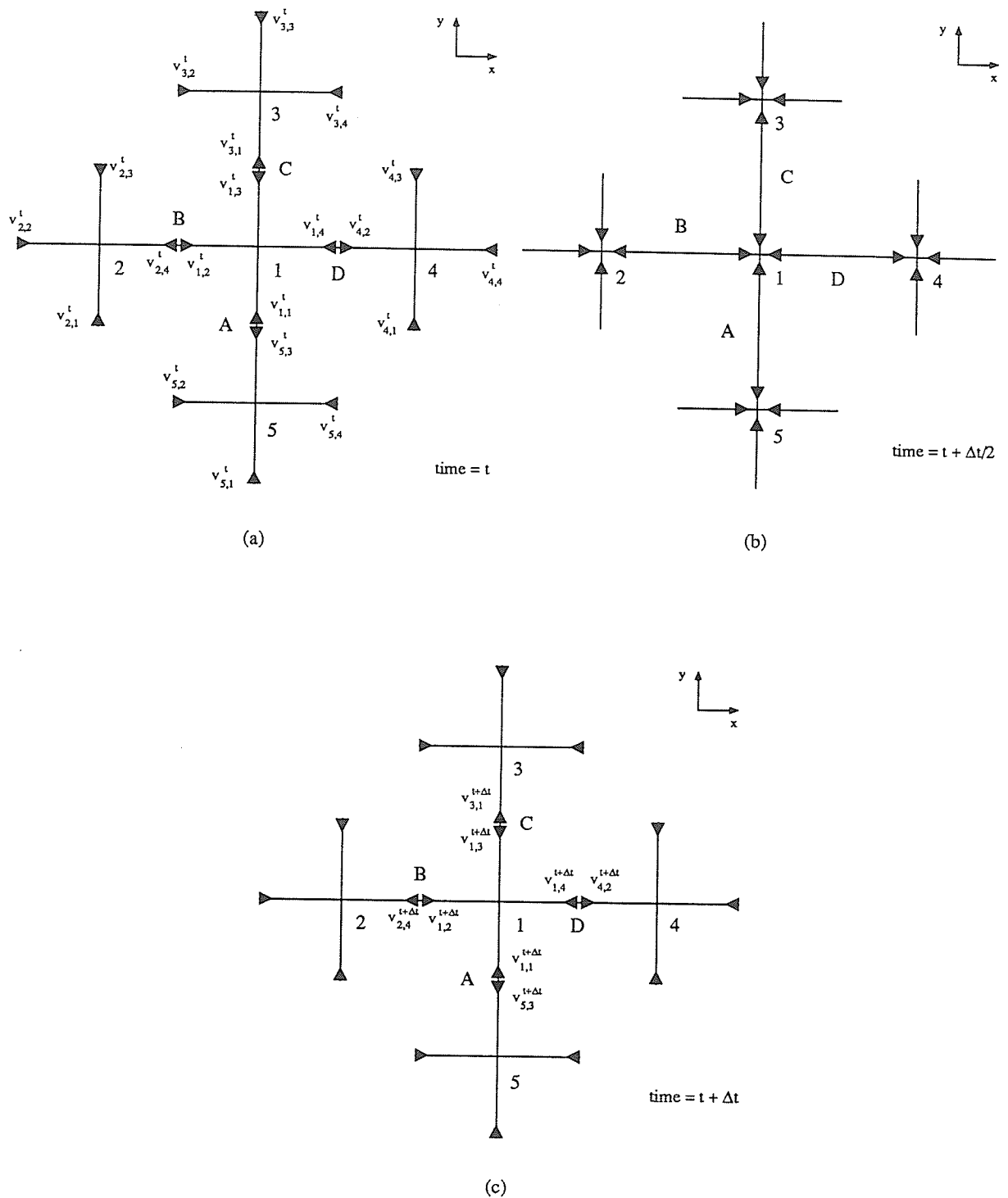


Figure 3.2: Operation of a group of five TLM nodes through one time step (a) time t , (b) time $t + \frac{\Delta t}{2}$, and (c) time $t + \Delta t$.

3.1.2.3. Equivalence of Modified TLM and FD-TD

In this section the difference approximations (3.7) to Maxwell's equations are obtained by examining the operation of the modified TLM scheme. Consider the group of two nodes shown in Figure 3.3. These two nodes are again considered to be a part of a larger TLM mesh. Node 1 is located at $x=x_o, y=y_o$, and node 2 is located at $x=x_o, y=y_o+\Delta l$. At time t (see Figure 3.3(a)), H_x^t is defined at $x=x_o, y=y_o+\Delta l/2$ as,

$$H_x^t(x_o, y_o + \frac{\Delta l}{2}) = v_{2,1}^t - v_{1,3}^t \quad (3.14)$$

At time $t=t+\Delta t/2$ (see Figure 3.3(b)), E_z at nodes 1 and 2 as,

$$E_z^{t+\frac{\Delta t}{2}}(x_o, y_o) = \frac{1}{2} \left[v_{1,1}^t + v_{1,2}^t + v_{1,3}^t + v_{1,4}^t \right] \quad (3.15)$$

and,

$$E_z^{t+\frac{\Delta t}{2}}(x_o, y_o + \Delta l) = \frac{1}{2} \left[v_{2,1}^t + v_{2,2}^t + v_{2,3}^t + v_{2,4}^t \right] \quad (3.16)$$

At time $t+\Delta t$ (see Figure 3.3(c)), the value of H_x at $x=x_o, y=y_o+\Delta l/2$ as,

$$H_x^{t+\Delta t}(x_o, y_o + \frac{\Delta l}{2}) = v_{2,1}^{t+\Delta t} - v_{1,3}^{t+\Delta t} \quad (3.17)$$

The incident pulses $v_{2,1}^{t+\Delta t}$ and $v_{1,3}^{t+\Delta t}$ are the reflected pulses from adjacent nodes at the previous time step,

$$v_{2,1}^{t+\Delta t}(\text{incident}) = v_{1,3}^t(\text{reflected}) \quad (3.18a)$$

$$v_{1,3}^{t+\Delta t}(\text{incident}) = v_{2,1}^t(\text{reflected}) \quad (3.18b)$$

These reflected pulses are expressed in terms of the incident pulses at time t at nodes 1 and 2 as,

$$v_{2,1}^{t+\Delta t} = v_{1,3}^t (\text{reflected}) = \frac{1}{2} \left[v_{1,1}^t + v_{1,2}^t - v_{1,3}^t + v_{1,4}^t \right] \quad (3.19a)$$

and

$$v_{1,3}^{t+\Delta t} = v_{2,1}^t (\text{reflected}) = \frac{1}{2} \left[-v_{2,1}^t + v_{2,2}^t + v_{2,3}^t + v_{2,4}^t \right] \quad (3.19b)$$

respectively. Therefore the value of $H_x^{t+\Delta t}(x_o, y_o + \frac{\Delta l}{2})$ can be written in terms of incident pulses on nodes 1 and 2 at time t . Substituting equations (3.19) into (3.17) yields,

$$H_x^{t+\Delta t}(x_o, y_o + \frac{\Delta l}{2}) = \frac{1}{2} \left[v_{1,1}^t + v_{1,2}^t - v_{1,3}^t + v_{1,4}^t + v_{2,1}^t - v_{2,2}^t - v_{2,3}^t - v_{2,4}^t \right]$$

Expanding the right hand side, to

$$H_x^{t+\Delta t}(x_o, y_o + \frac{\Delta l}{2}) = v_{2,1}^t - v_{3,1}^t + \frac{1}{2} \left[v_{1,1}^t + v_{1,2}^t + v_{1,3}^t + v_{1,4}^t - v_{2,1}^t - v_{2,2}^t - v_{2,3}^t - v_{2,4}^t \right]$$

and recognizing expressions for H_x at time t and E_z at time $t + \frac{\Delta t}{2}$ yields

$$H_x^{t+\Delta t}(x_o, y_o + \frac{\Delta l}{2}) = H_x^t(x_o, y_o + \frac{\Delta l}{2}) - \left[E_z^{t+\frac{\Delta t}{2}}(x_o, y_o + \Delta y) - E_z^{t+\frac{\Delta t}{2}}(x_o, y_o) \right] \quad (3.20)$$

which is equivalent to the difference approximation (3.7a) with $\mu=1$ and $\Delta t/\Delta y=1$.

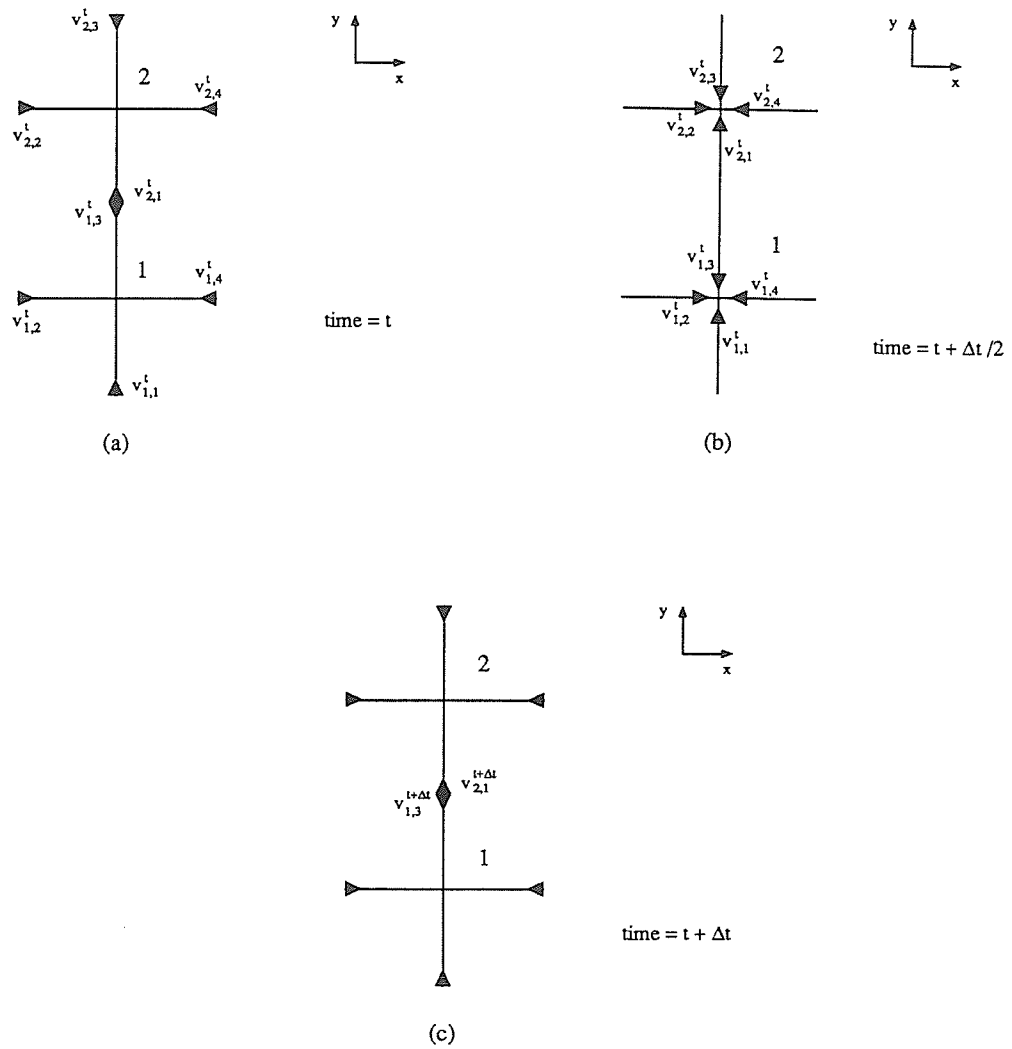


Figure 3.3: Operation of two nodes adjacent in the y direction at (a) time t , (b) time $t + \frac{\Delta t}{2}$, and (c) time $t + \Delta t$

Equation (3.7b) is obtained in the same manner, by considering two nodes adjacent to each other in the x direction. $H_y^{t+\Delta t}(x_o + \frac{\Delta l}{2}, y_o)$ can be written in terms of incident pulses at time t . Expressions for $H_y^t(x_o + \frac{\Delta l}{2}, y_o)$, $E_z^{t+\frac{\Delta t}{2}}(x_o + \Delta l, y_o)$, and $E_z^{t+\frac{\Delta t}{2}}(x_o, y_o)$

are written in terms of incident impulses at time t and yield,

$$H_y^{t+\Delta t}(x_o + \frac{\Delta l}{2}, y_o) = H_y^t(x_o + \frac{\Delta l}{2}, y_o) + \left[E_z^{t+\frac{\Delta t}{2}}(x_o + \Delta l, y_o) - E_z^{t+\frac{\Delta t}{2}}(x_o, y_o) \right] \quad (3.21)$$

which is equivalent to the difference approximation (3.6b) again with $\mu=1$ and $\frac{\Delta t}{\Delta y}=1$.

Equation (3.7c) is obtained by considering a group of five nodes configured as in Figure 3.2. The electric field at node 1 at time $t+\Delta t/2$ is

$$E_z^{t+\frac{\Delta t}{2}}(x_o, y_o) = \frac{1}{2} \left[v_{1,1}^t + v_{1,2}^t + v_{1,3}^t + v_{1,4}^t \right] \quad (3.22)$$

and the electric field at node 2 at time $t-\Delta t/2$ is

$$E_z^{t-\frac{\Delta t}{2}}(x_o, y_o) = \frac{1}{2} \left[v_{1,1}^{t-\Delta t} + v_{1,2}^{t-\Delta t} + v_{1,3}^{t-\Delta t} + v_{1,4}^{t-\Delta t} \right] \quad (3.23)$$

A property of the scattering matrix of the TLM node is either incident or reflected pulses can be used in the definition for the electric field. Use of either will result in identical E_z values. In expressions (3.22) and (3.23) the pulses are considered as reflected pulses. The reflected pulses on node 1 at time $t-\Delta t$ become incident pulses on adjacent nodes at time t .

$$v_{5,3}^t(\text{incident}) = v_{1,1}^{t-\Delta t}(\text{reflected}) \quad (3.24a)$$

$$v_{2,4}^t(\text{incident}) = v_{1,2}^{t-\Delta t}(\text{reflected}) \quad (3.24b)$$

$$v_{3,1}^t(\text{incident}) = v_{1,3}^{t-\Delta t}(\text{reflected}) \quad (3.24c)$$

$$v_{4,2}^t(\text{incident}) = v_{1,4}^{t-\Delta t}(\text{reflected}) \quad (3.24d)$$

The electric field $E_z^{t+\frac{\Delta t}{2}}$ at node 1 is expressed in terms of incident pulses on adjacent nodes as

$$E_z^{t+\frac{\Delta t}{2}}(x_o, y_o) = \frac{1}{2} \left[v_{4,2}^t + v_{3,1}^t + v_{2,4}^t + v_{5,3}^t \right] \quad (3.25)$$

The difference between $E_z^{t+\frac{\Delta t}{2}}(x_o, y_o)$ and $E_z^{t-\frac{\Delta t}{2}}(x_o, y_o)$ can be written as

$$\begin{aligned} E_z^{t+\frac{\Delta t}{2}}(x_o, y_o) - E_z^{t-\frac{\Delta t}{2}}(x_o, y_o) = \\ \frac{1}{2} \left[v_{1,1}^t + v_{1,2}^t + v_{1,3}^t + v_{1,4}^t - v_{5,3}^t - v_{2,4}^t - v_{3,1}^t - v_{4,2}^t \right] \end{aligned} \quad (3.26)$$

Using the definitions for magnetic field quantities in (3.12), (3.26) can be re-written in terms of field quantities alone as,

$$\begin{aligned} E_z^{t+\frac{\Delta t}{2}}(x, y) - E_z^{t-\frac{\Delta t}{2}}(x, y) = \frac{1}{2} \left[H_y^t(x + \frac{\Delta l}{2}, y) - H_y^t(x - \frac{\Delta l}{2}, y) \right] \\ - \frac{1}{2} \left[H_x^t(x, y + \frac{\Delta l}{2}) - H_x^t(x, y - \frac{\Delta l}{2}) \right] \end{aligned} \quad (3.27)$$

which is equivalent to (3.7c) with $\epsilon=2$ and $\Delta t/\Delta l=1$. As expected, the grid of transmission lines simulates a space characterized by $\mu=1$, $\epsilon=2$. The apparent violation of the stability criterion $\frac{\Delta t}{\Delta y} \leq \frac{1}{\sqrt{2}c}$ required by the FD-TD algorithm [41] is discussed in section 1.3.3 of this chapter.

3.1.3. Comparison By Propagation Analysis

The previous sections have shown that the TLM method can be operated in a manner that will satisfy difference approximations to Maxwell's equations. In this section the characteristic equations governing wave propagation in the TLM and FD-TD methods are compared. In general, time domain numerical methods capable of simulating wave propagation do not propagate waves ideally, because approximations are required in the formulation of the method. These errors are either dispersive (waves at different frequencies travel at different speeds causing waveforms to change shape as

they propagate) or dissipative (waves are attenuated as they propagate) [50]. Both errors can be present in a time domain propagation model, however the TLM and FD-TD methods cause dispersive errors only. A characteristic equation can be derived from the propagation model that governs wave propagation in the method. For non-dissipative models this equation is called the dispersion relation. A general discussion of dispersion relations for finite difference models of the wave equation can be found in [50].

The dispersion relation is derived by substituting an exact solution to the governing differential equation into the approximate equation of the model. For the case of finite difference approximations to the wave equation, representation of an ideal plane wave travelling at an arbitrary direction is substituted into the difference approximation to the wave equation. The dispersion relations for both the FD-TD and TLM methods are derived for an arbitrary medium. From these relations it can again be shown under what conditions the propagation mechanisms are identical.

3.1.3.1. Dispersion Relation of FD-TD Method

Maxwell's equations for two dimensional TE propagation as given in (3.3) can be combined to yield the lossy wave equation,

$$\frac{\partial^2 E_z}{\partial x^2} + \frac{\partial^2 E_z}{\partial y^2} = \sigma \mu \frac{\partial E_z}{\partial t} + \epsilon \mu \frac{\partial^2 E_z}{\partial t^2} \quad (3.28)$$

The above differential equation can be discretized using the difference expressions,

$$\frac{\partial^2 f}{\partial \eta^2} = \frac{f(\eta + \frac{\Delta\eta}{2}) - 2f(\eta) + f(\eta - \frac{\Delta\eta}{2})}{\Delta\eta^2} \quad O(\Delta\eta)^2 \quad (3.29a)$$

and

$$\frac{\partial f}{\partial \eta} = \frac{f(\eta + \frac{\Delta \eta}{2}) - f(\eta - \frac{\Delta \eta}{2})}{\Delta \eta} \quad \mathcal{O}(\Delta \eta)^2 \quad (3.29b)$$

Applying (3.29) to both space and time derivatives in (3.28) and using equal space increments $\Delta x = \Delta y = \Delta l$ equation (3.28) becomes,

$$\begin{aligned} & \frac{E_z^{t_o}(x_o + \Delta l, y_o) - 2E_z^{t_o}(x_o, y_o) + E_z^{t_o}(x_o - \Delta l, y_o)}{\Delta l^2} \\ & + \frac{E_z^{t_o}(x_o, y_o + \Delta l) - 2E_z^{t_o}(x_o, y_o) + E_z^{t_o}(x_o, y_o - \Delta l)}{\Delta l^2} \\ & = \sigma \mu \frac{E_z^{t_o + \Delta t}(x_o, y_o) - E_z^{t_o - \Delta t}(x_o, y_o)}{2\Delta t} \\ & + \epsilon \mu \frac{E_z^{t_o + \Delta t}(x_o, y_o) - 2E_z^{t_o}(x_o, y_o) + E_z^{t_o - \Delta t}(x_o, y_o)}{\Delta t^2} \end{aligned} \quad (3.30)$$

A solution of equation (3.28) can be written as

$$E_z = e^{j\omega t + \gamma \cos \phi x + \gamma \sin \phi y} \quad (3.31)$$

which represents a plane wave traveling through the medium characterized by a complex propagation constant $\gamma = \alpha + j\beta$ at an angle ϕ to the x axis. Inserting solution (3.31) into the difference approximation (3.30), along with cancelling common terms and using trigonometric identities, the following relationship is obtained

$$\sinh^2 \frac{\gamma \cos \phi \Delta l}{2} + \sinh^2 \frac{\gamma \sin \phi \Delta l}{2} = j \frac{\sigma \mu \Delta l^2}{\Delta t} \frac{\sin \omega \Delta t}{4} - \epsilon \mu \frac{\Delta l^2}{\Delta t^2} \sin^2 \frac{\omega \Delta t}{2} \quad (3.32)$$

For the case of a non conductive medium ($\alpha = 0$), (3.32) reduces to the familiar result [50].

$$\sin^2 \frac{\beta \cos \phi \Delta l}{2} + \sin^2 \frac{\beta \sin \phi \Delta l}{2} = \epsilon \mu \frac{\Delta l^2}{\Delta t^2} \sin^2 \frac{\omega \Delta t}{2} \quad (3.33)$$

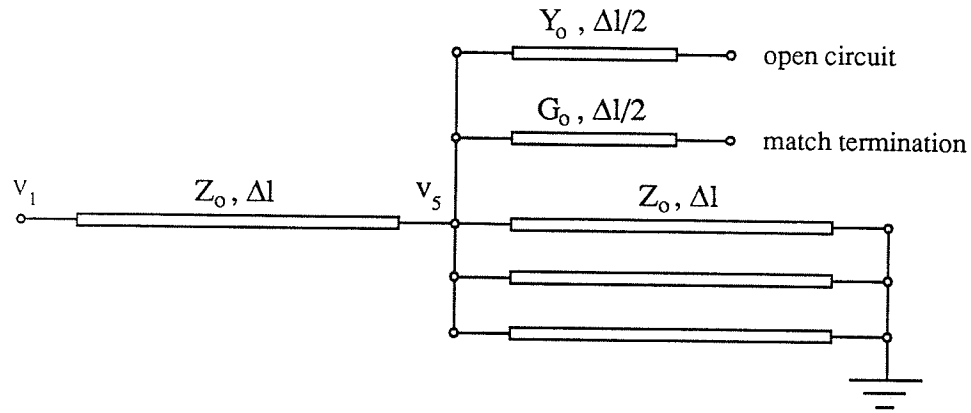
The above relationships govern the manner in which the second order leap frog

scheme propagates waves.

3.1.3.2. Propagation Analysis of the TLM Node

Johns and Brewitt-Taylor [19] have applied the concept of determining the dispersion relation to TLM models and have referred to it as propagation analysis. The same technique that is used to calculate dispersion relations is applied, but instead of substituting the analytical solution of the lossy wave equation into a difference approximation, it is substituted into an equation governing the behavior of voltages on the transmission line model. Johns and Brewitt-Taylor have performed propagation analysis of a two dimensional shunt node without permittivity and conductivity stubs [19]. In this section propagation analysis of a two dimensional shunt node complete with permittivity and conductivity stubs is performed. As well, the analysis is given in terms of basic transmission line circuit theory, simplifying the analysis of Johns and Brewitt-Taylor [19].

The two dimensional node complete with permittivity and loss stubs is shown in Figure 2.6. In order to occupy the same area of space as the difference approximation (3.29) the arms of the node are extended to the centre of adjacent nodes. Considering the operation of this node in a time harmonic situation, the node can be analyzed using simple transmission line theory and superposition. Exciting the node with v_1 and suppressing nodes 2,3, and 4, the equivalent circuit of the node is shown in Figure 3.4.



or,

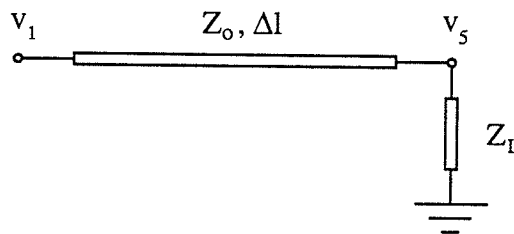


Figure 3.4: Equivalent circuit of TLM shunt node loaded with permittivity and loss stubs. All branches except branch 1 are terminated in a short circuit. Note that the intrinsic impedance Z_o is assumed to equal 1.0

The load impedance Z_L is made up of three short circuit stubs of length Δl and unit characteristic impedance, one open circuit stub of length $\Delta l/2$ and characteristic admittance Y_o , and one match terminated line with a characteristic admittance of G_o , all in parallel. The impedance Z_L is expressed as,

$$Z_L = \left[\frac{3}{j \tan \beta \Delta l} + j Y_o \tan \frac{\beta \Delta l}{2} + G_o \right]^{-1} \quad (3.34)$$

Simple transmission line theory can be used to write [18],

$$v_1 = v_5^1 \left[\cos \beta \Delta l + \frac{j \sin \beta \Delta l}{Z_L} \right] \quad (3.35a)$$

or solving for v_5^1 ,

$$v_5^1 = \frac{v_1}{\left[\cos \beta \Delta l + \frac{j \sin \beta \Delta l}{Z_L} \right]} \quad (3.35b)$$

Noting the symmetry of the node, and applying the principle of superposition, the voltage v_5 can be expressed as a summation of the voltages v_5^n as,

$$v_5 = \sum_{n=1}^4 v_5^n \quad (3.36a)$$

where $v_5^n = \frac{v_n}{\left[\cos \beta \Delta l + \frac{j \sin \beta \Delta l}{Z_L} \right]}$ which leads to

$$\sum_{n=1}^4 v_n = v_5 \left[\cos \beta \Delta l + \frac{j \sin \beta \Delta l}{Z_L} \right] \quad (3.36b)$$

and substituting the expression for Z_L and using trigonometric identities equation (3.36) become,

$$\sum_{n=1}^4 v_n = v_5 \left[4 \sin \beta \Delta l - 2 Y_o \sin^2 \frac{\beta \Delta l}{2} + j G_o \sin \beta \Delta l \right] \quad (3.37)$$

Equation (3.37) governs the behavior of voltages on the transmission line model. A plane wave traveling through space at an angle ϕ to the x axis is given by (3.31). This plane wave travels through the TLM mesh as a voltage wave with the exact solution being

$$V_z = V_o e^{j\omega t + \gamma \cos\phi x + \gamma \sin\phi y} \quad (3.38)$$

Substituting (3.38) into (3.37) along with cancelling common terms and using trigonometric identities, the following expression is obtained

$$\sinh^2 \frac{\gamma \cos\phi \Delta l}{2} + \sinh^2 \frac{\gamma \sin\phi \Delta l}{2} = j \frac{G_o}{4} \sin\beta \Delta l + 2 \left(1 + \frac{Y_o}{4} \right) \sin^2 \frac{\beta \Delta l}{2} \quad (3.39)$$

where $\gamma = \alpha + j\beta$ and G_o and Y_o are defined in (3.8) and (3.9). If a medium with zero conductivity is considered ($\alpha = G_o = 0$) (3.39) reduces to the result obtained by Johns and Brewitt-Taylor [19].

$$\sin^2 \frac{\beta \cos\phi \Delta l}{2} + \sinh^2 \frac{\beta \sin\phi \Delta l}{2} = 2 \left(1 + \frac{Y_o}{4} \right) \sin^2 \frac{\beta \Delta l}{2} \quad (3.40)$$

3.1.3.3. Equivalence of Propagation Characteristics

Although the propagation characteristics of both the two dimensional TLM node and FD-TD method are well known [19],[20], [50], the equivalence between the two methods has not been established. In this section the equivalence between dispersion relations is established. In addition, the difference between modelling philosophies and the implications regarding the FD-TD stability factor [41] are discussed. Examining equations (3.39) and (3.31), the conditions under which the TLM and FD-TD correspond are defined by,

$$\begin{aligned} \mu &= 1 \\ \epsilon &= 2 \left(1 + \frac{Y_o}{4} \right) \\ \sigma &= \frac{G_o}{\mu} \end{aligned}$$

$$\text{and } \frac{\Delta t}{\Delta l} = 1 \quad (3.41)$$

From the conditions above it appears that the TLM algorithm violates the stability criterion (3.6) for FD-TD simulations [41]. This should not cause any concern as the stability of the TLM algorithm has been established [27]. The apparent violation of the stability criterion is caused by the difference in modelling philosophies between the two methods. In TLM simulations the reference medium to which media properties are normalized is that of the elemental transmission lines. The medium modelled by the mesh does not represent a normalized free space, the properties of the elemental transmission line represent a normalized free space. In expression (3.6), c refers to the free space velocity of waves through the FD-TD mesh, and for a normalized simulation space $c=1$. However, in a TLM mesh the free space velocity of waves is $c=1/\sqrt{2}$. The stability criterion as applied to TLM simulations should be written as,

$$\frac{\Delta t}{\Delta l} \leq 1 \quad (3.42)$$

and therefore FD-TD and TLM algorithms correspond when the FD-TD algorithm is operated at the upper limit of its stability range.

Operating the FD-TD algorithm at its stability limit has benefits in that the amount of dispersion introduced by the algorithm is minimum for all directions of propagation [51]. As well, for certain test cases, simulations indicate that accuracy is optimal [52].

Johns has discussed the significance of comparisons and the philosophy behind the two methods [48]. The two methods are distinct in that they are based on different ideas. The TLM method is based on a model for wave propagation realized as a mesh of intersecting transmission lines and the FD-TD method is based on mathematical differencing. It is interesting to find that distinct concepts produce equivalent numerical methods.

3.2. TLM and Beregeron's Method

Beregeron's method is theoretically similar to the TLM method as it is based on the equivalent circuit of Maxwell's equations. The TLM method provides an exact solution to a transmission line model, while Beregeron's method provides a numerical solution to a lumped element model using a trapezoid rule integration scheme [17]. Applications of this method have been in the area of transient analysis of microstrip discontinuities [17],[53],[54] and more recently to investigate the behavior of perfectly conducting targets coated with absorbing materials [55],[44].

Johns and Brewitt-Taylor have performed propagation analysis of both transmission line and the lumped element models of Maxwell's equations [19].

Consider the lumped element and transmission line models in Figure 2.2(a) and Figure 2.4 respectively. The nodal equations for voltages on the lumped element and transmission line models are [19] respectively,

$$\sum_{n=1}^4 v_n = j\omega\mu\Delta l^2(\sigma + j\omega\epsilon)v_5 \quad (3.43)$$

$$\sum_{n=1}^4 v_n = 8\sinh^2\left(\frac{\gamma\Delta l}{2}\right)v_5 \quad (3.44)$$

where,

$$\gamma^2 = \frac{j\omega\mu}{2}(\sigma + j\omega\epsilon)$$

If the \sinh^2 term in (3.44) is expanded into an infinite series and only the first term of the infinite series is retained, equation (3.44) is reduced to (3.43). This implies the lumped element model is an approximation of the transmission line model. Substituting the exact solution of a plane wave travelling through the medium (as was done in sections 4 and 5) the dispersion relations are obtained for the lumped element network,

$$\sin^2 \frac{\pi c \Delta l}{\lambda v} \cos \phi + \sin^2 \frac{\pi c \Delta l}{\lambda v} \sin \phi = \left[\frac{\pi \Delta l}{\lambda} \right] \quad (3.45)$$

and for the transmission line network,

$$\sin^2 \frac{\pi c \Delta l}{\lambda v} \cos \phi + \sin^2 \frac{\pi c \Delta l}{\lambda v} \sin \phi = 2 \sin^2 \frac{\pi \Delta l}{\sqrt{2} \lambda} \quad (3.46)$$

To examine propagation parallel to an axis of the mesh, $\phi=0$ is substituted into (3.45) and (3.46). From the resulting equations a ratio of v/c can be found for the lumped element network,

$$\frac{v}{c} = \pi \frac{\Delta l}{\lambda} \frac{1}{\sin^{-1}(\pi \frac{\Delta l}{\lambda})} \quad (3.47)$$

and the transmission line network,

$$\frac{v}{c} = \pi \frac{\Delta l}{\lambda} \frac{1}{\sin^{-1} \left[\sqrt{2} \sin \left(\frac{\pi \Delta l}{\sqrt{2} \lambda} \right) \right]} \quad (3.48)$$

The characteristics (3.47) and (3.48) are plotted in Figure 3.5. To examine diagonal propagation through the mesh, $\phi=45^\circ$ is substituted into (3.45) and (3.46). From the resulting equations a ratio of v/c can be found for the lumped element network,

$$\frac{v}{c} = \frac{\pi \Delta l}{\sqrt{2} \lambda} \frac{1}{\sin^{-1} \left[\frac{\pi \Delta l}{\sqrt{2} \lambda} \right]} \quad (3.49)$$

and the transmission line network,

$$\frac{v}{c} = 1 \quad (3.50)$$

The characteristics (3.49) and (3.50) are plotted in Figure 3.6.

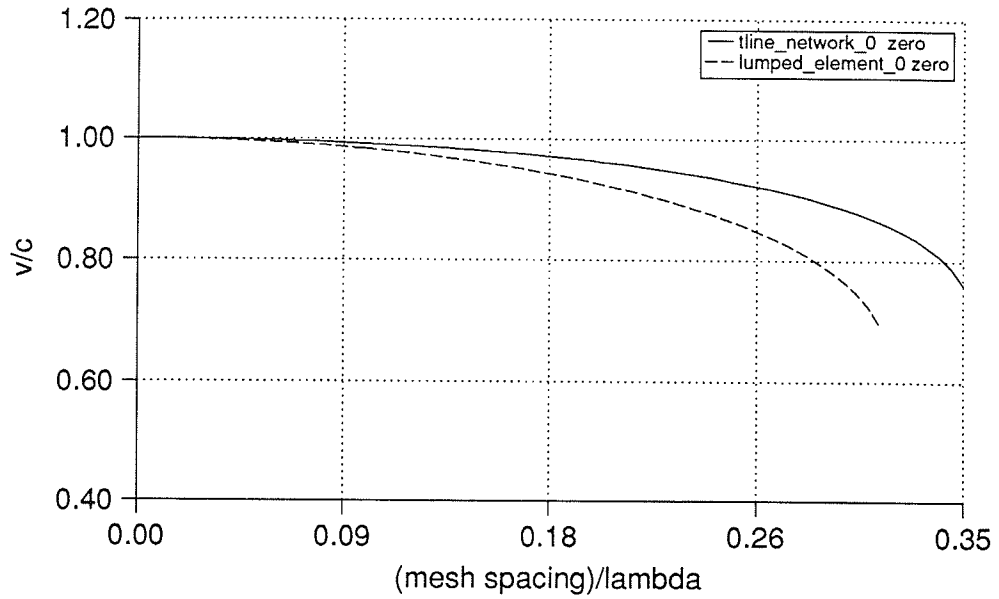


Figure 3.5: Ratio of velocity of propagation and free space velocity for the *t*-line and lumped element network for diagonal propagation

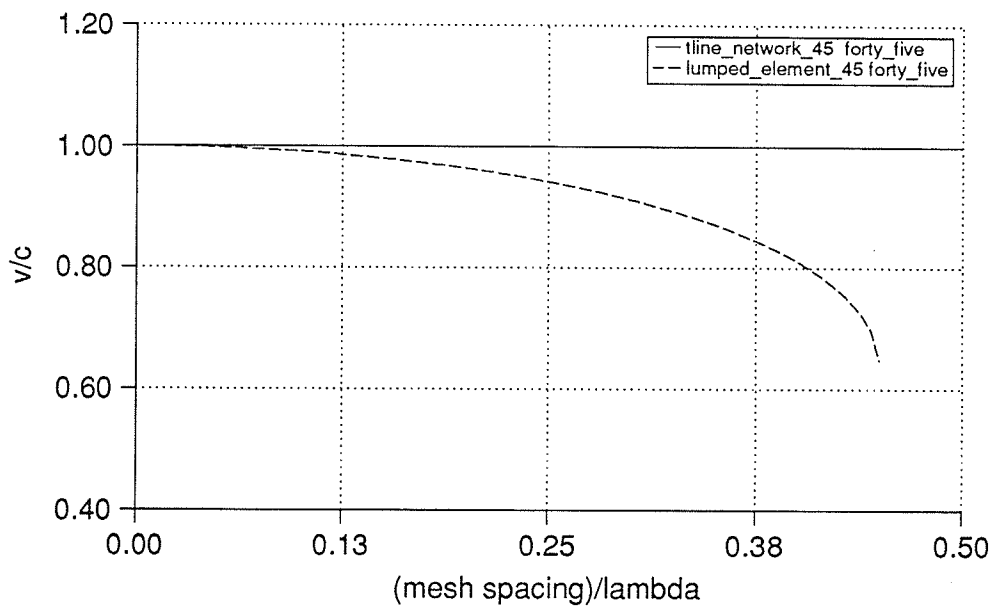


Figure 3.6: Ratio of velocity of propagation and free space velocity in *t*-line and lumped element network propagation parallel to a mesh axis

Figure 3.5 and Figure 3.6 indicate waves travelling in the transmission line network experience less dispersion than those in the lumped element network. For propagation at 45° to a mesh axis, waves in the transmission line network travel with no dispersion at all. In general, for all angles of propagation the transmission line model is consistently more accurate than the lumped element model [19].

Chapter 4

Application of the TLM Method to Scattering Problems

This chapter outlines the application of the TLM method to two dimensional scattering problems. In the first section of this chapter, the configuration of the mesh is discussed. To accurately model incident and scattered fields, a method that separates scattered fields from total fields is implemented. This scheme has been used in FD-TD programs [4],[5] and is reformulated in terms of a time domain equivalence principle in order to achieve implementation into TLM simulations. In the second section, absorbing boundary conditions are presented. An absorbing boundary condition to match terminate a TLM mesh is developed, however, it does not lend itself to practical implementation for an arbitrary scattering problem. Absorbing boundary conditions for use with FD-TD simulations have been extensively investigated. Since the relationship between the FD-TD and TLM methods has been discussed in the previous chapter, one class of FD-TD absorbing boundary conditions will be applied to TLM simulations. The last section of this chapter discusses the calculation of scattered far field patterns from near field patterns. The efficiency of various techniques applied to calculated frequency domain scattered far field patterns is also considered.

4.1. Configuration of the Mesh

The problem considered in this thesis is shown in Figure 4.1. The scatterer is considered as infinite in the z direction and illuminated by an E polarized plane wave. The fields in the region at an arbitrary point in time consist of both scattered and incident fields (i.e., $E_z^{total} = E_z^{scattered} + E_z^{incident}$). Only a z component of the electric field and x and y components of the magnetic field are present. The presence of these field components has been described in previous chapters as TE propagation because the electric field is transverse to the direction of propagation [56]. The situation described in Figure 4.1 is referred to as TM scattering because the magnetic field is transverse to the axis of the scatterer [57]. The outline of the scatterer is given by the contour S in Figure 4.1. A perfectly conducting cylinder is modelled by placing reflection coefficients ($\Gamma = -1.0$) to best fit the contour S . Dielectric cylinders are modelled by loading nodes within the contour S with permittivity stubs. The incident plane wave is modelled by placing impulses along a line $x = x_e$.

To model the problem in Figure 4.1, the TLM mesh must be truncated to limit the infinite simulation space surrounding the scatterer along the lines $x = x_1$, $x = x_2$, $y = y_1$ and $y = y_2$. One possible choice is to use absorbing conditions on all exterior boundaries to accurately model the outgoing scattered field. However, along the boundaries $y = y_1$, $y = y_2$ absorbing boundary conditions would interfere with the incident plane wave. An ideal plane wave travelling along the x axis is infinite in extent in the y direction, therefore magnetic walls are required along $y = y_1$ and $y = y_2$. Absorbing boundary conditions placed along all exterior boundaries accurately models the scattered fields but interferes with the incident field. Therefore, this formulation models scattering by something other than an ideal plane wave. Clearly, if the incident field is inaccurate the final results will not be accurate.

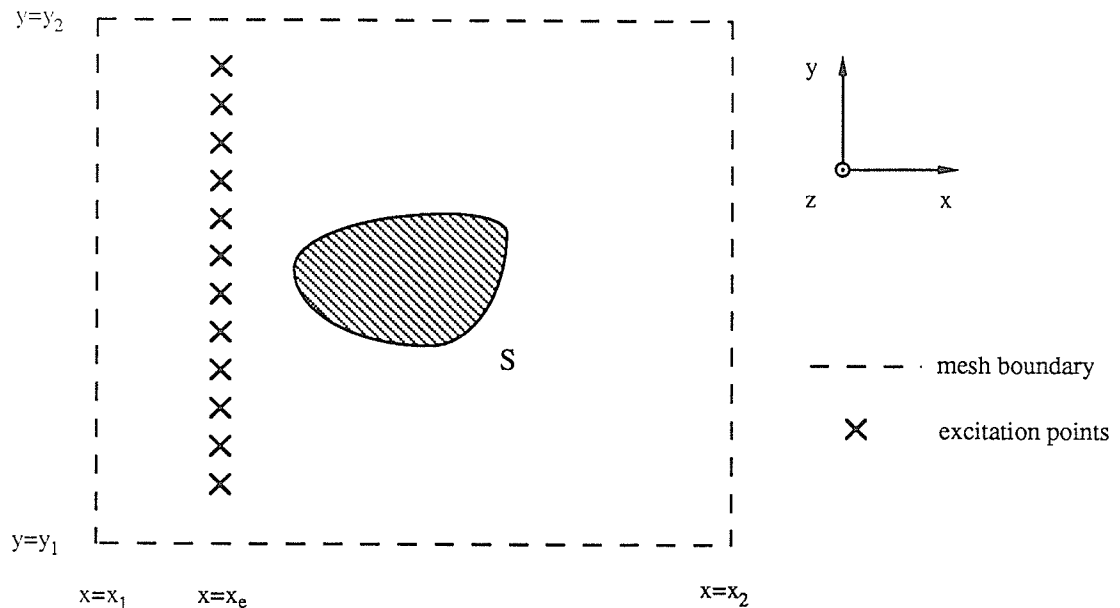


Figure 4.1: Two dimensional scattering problem: arbitrary shape, arbitrary material properties.

A second choice of boundary conditions is to place magnetic walls along $y=y_1$, $y=y_2$ and absorbing boundary conditions along $x=x_1$, $x=x_2$. This formulation accurately models an incident plane wave, however the scattered fields are not absorbed by the magnetic walls and inaccurate scattered fields result. Ney and Yue [40] have used this scheme to model two dimensional scattering problems. To reduce the errors introduced to the scattered field by the magnetic walls, the simulation space was extended in the y direction. The mesh was made sufficiently large so that reflections from the magnetic walls do not reach the output points before the iteration process stops. This scheme provides accurate modelling at the expense of cpu time and memory storage requirements. A formulation of the TLM method is required that allows excitation of the scatterer with an accurate incident field while applying absorbing boundary conditions to only the scattered fields.

A formulation of this type has been developed for the FD-TD method by Merewether *et al* [58] and by Umashankar and Taflove [5]. Merewether describes the formulation as a numerical Huygen's source scheme and Umashankar and Taflove describe the formulation as a separation of total and scattered fields. The implementations above are developed explicitly for use with FD-TD simulations and are based on the equivalence principle. Although the relationship between TLM and FD-TD has been discussed in the previous Chapter, due to the difference between the basic algorithms (difference approximations versus scattering of impulses off transmission line junctions) the formulations in the references given above are not applicable to TLM simulations. Harrington provides a description of the equivalence principle for time harmonic steady state fields [57], including a circuit theory analogue. Because the TLM method is essentially a time domain circuit simulation, the purpose of the next section is to develop an analogue of the equivalence principle applicable to the excitation of electrical networks in the time domain.

4.1.1. Time Domain Equivalence Principle

Consider the circuit shown in Figure 4.2 consisting of a source network S connected to a load network L by n ideal transmission lines. Examining the excitation of this network allows the development of the required formulation. To allow simplified adaptation to TLM simulations, the following assumptions regarding the nature of the network are made:

- 1) the load network L consists of passive frequency independent components,
- 2) the source network S consists of passive frequency independent components and ideal independent voltage sources, and
- 3) the ideal independent voltage sources in S produce impulsive excitation.

If the sources in S are energized at time $t=0$, at a future point in time, pulses will be travelling throughout both networks and between them on the n ideal transmission lines. An impulse travelling from L to S is considered as a reflected impulse, and on the j^{th} transmission line these impulses are defined as $v_j^r(t)$. An impulse travelling from S to L on the j^{th} transmission line is a superposition of impulses originating from the sources within S and re-reflections of impulses $v_j^r(t)$ reflected back to L . This train of impulses travelling from S to L is defined as $v_j^f(t)$.

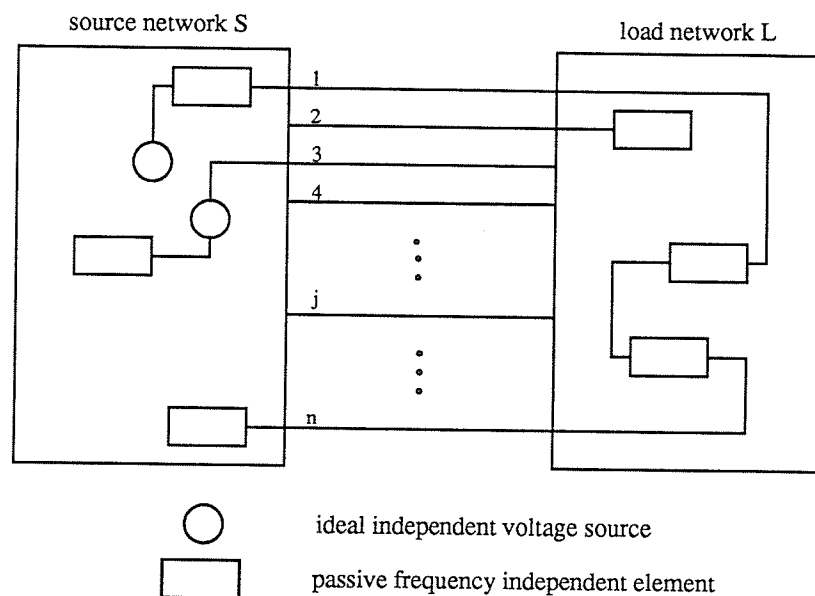


Figure 4.2: *Electrical network used to formulate the time domain equivalence principle.*

Two methods of providing an equivalent excitation to the load network L are considered. Both require that the impulse trains, $v_j^r(t)$ and $v_j^f(t)$ be known from either previous simulations or a simultaneous simulation.

Method 1:

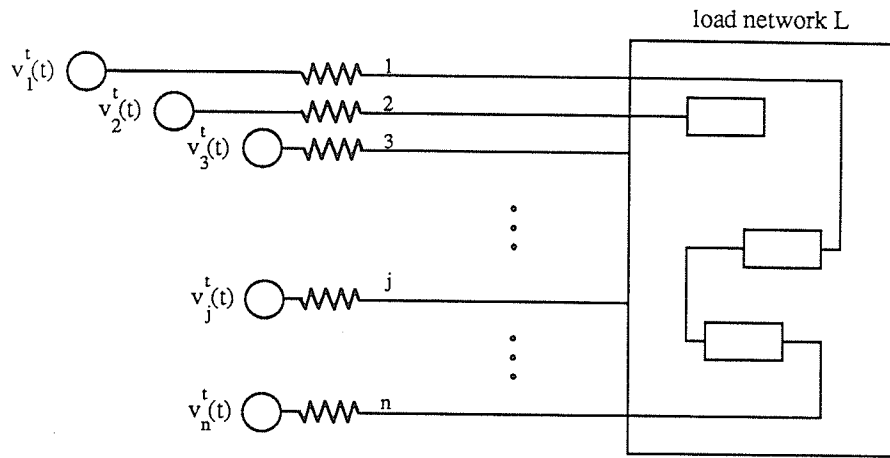
The source network S is removed and matched sources are connected to the n transmission lines as shown in Figure 4.3(a). The source function used to excite the j^{th} line is $v_j^f(t)$, for all n transmission lines. A matched source is used to absorb any pulses reflected by L . The re-reflection of these pulses from S in the original problem back into L are accounted for by the source functions $v_j^f(t)$.

Method 2:

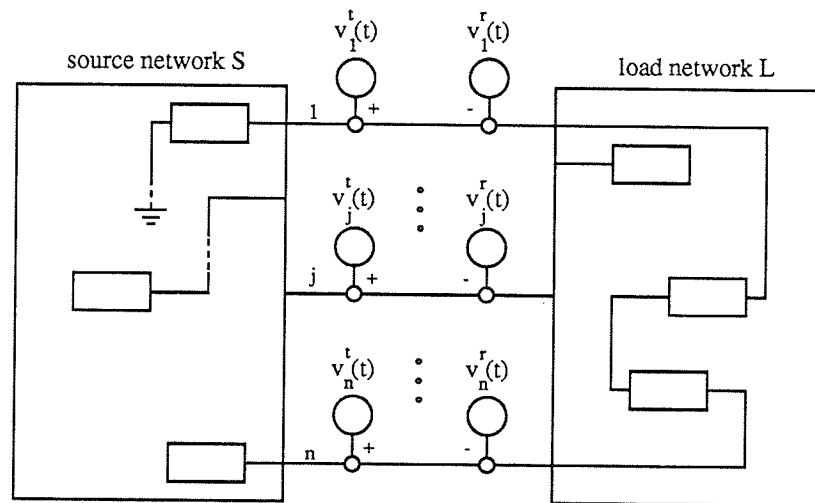
An alternative excitation of the load network L can be provided with the source network connected to the n transmission lines as shown in Figure 4.3(b). The independent sources in S are turned off, leaving S a passive network. To excite the load network L , source functions of $v_j^f(t)$ and $v_j^r(t)$ are applied to each of the n transmission lines ($j=1, 2, \dots, n$). The source functions are applied such that at a time t_o ,

- (i) a pulse travelling from S to L on the j^{th} line has the value $v_j^f(t_o)$ added to it, and
- (ii) a pulse travelling from L to S on the j^{th} line has the value $v_j^r(t_o)$ subtracted from it.

Applying (i) and (ii) at every time step and on every line, this method provides an equivalent excitation of the load network L . Operation (ii) has the same effect as the matched source impedances used in Method 1. The voltage in S is zero at every time step since no impulses originate from S (the independent sources have been turned off), and any impulse entering S is eliminated by operation (ii). These reflected pulses are eliminated because the re-reflections are already accounted for by the source $v_j^f(t)$. Although the voltage throughout the source network is zero, an explanation of why it remains connected in the circuit will become obvious when TLM scattering simulations are discussed.



(a)



(b)

Figure 4.3: Equivalent excitation of the network in Figure 4.2 (a) with the source network disconnected and matched sources applied to the n transmission lines and, (b) with the source network connected and operations (i) and (ii) applied to the n transmission lines.

Both of the methods described are capable of applying an excitation equivalent to that in the original problem, and can be considered as circuit theory analogues of a

time domain equivalence principle.

4.1.2. Use of Equivalent Excitation in TLM Simulations

Consider the TLM mesh in Figure 4.4 in which magnetic walls are placed along the boundaries $y=y_1$, $y=y_2$ and absorbing boundary conditions along $x=x_1$, $x=x_2$. An ideal plane wave can be generated in this mesh by applying impulses as initial conditions along a line $x=x_e$ from $y=y_1$ to $y=y_2$. The TLM mesh consists of ideal transmission lines which are passive non dispersive circuit elements and the excitation applied as initial conditions can be considered as ideal independent voltage sources placed at nodes in the mesh. The TLM mesh can be partitioned into two regions. Region I containing all of the excitation points and Region II consisting of the remaining portion of the mesh. Regions I and II correspond to the source and load networks respectively of the circuit in Figure 4.2. The only restrictions on the placement and location of the two regions is that the union of the two regions is the entire mesh, the intersection of the two regions is empty, and Region I contains all excitation points. Since the TLM mesh of Figure 4.4 satisfies the assumptions 1) - 3) (described in section 1.1 of this chapter), the methods of equivalent excitation can be applied.

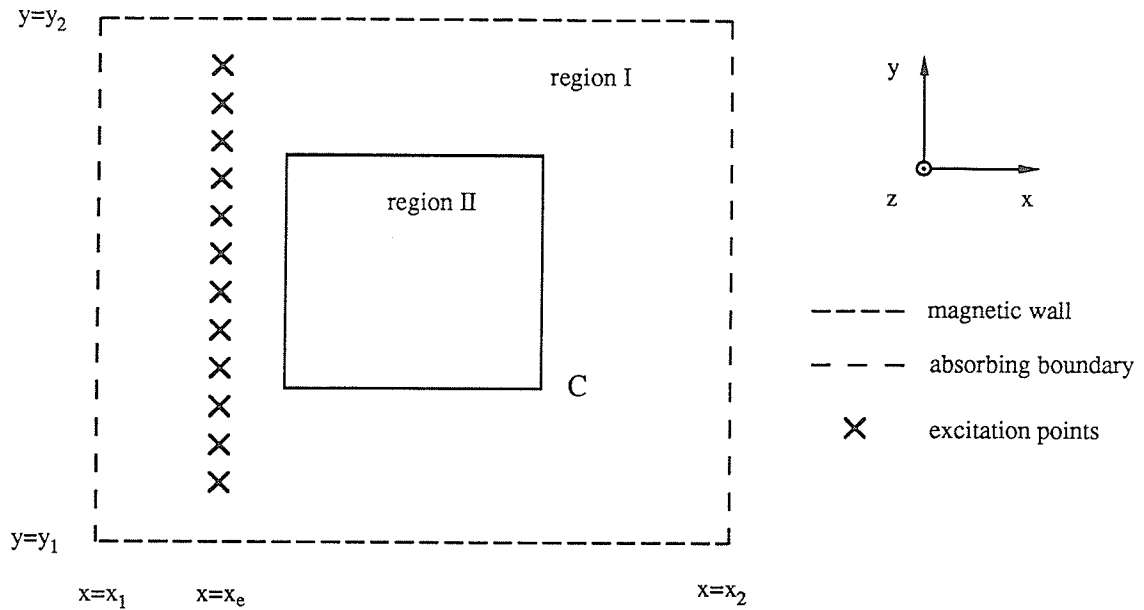


Figure 4.4: TLM simulation of a plane wave propagating through free space.

Regions I and II are separated by the contour C (as shown in Figure 4.4) which intersects the elemental transmission lines at midpoints between nodes (n intersections exist around C). At every iteration step two voltage impulses cross C, one passing from Region I to II, the other passing from Region II to I. On the j^{th} elemental transmission line crossing C, the impulses passing from Region I to II and from Region II to I represent the signals $v_j^i(t)$ and $v_j^r(t)$ respectively. These signals are required in the equivalent excitation of Region II. These two signals can be obtained by two methods. The first method is to run the simulation of Figure 4.4 and store the values of $v_j^i(t)$ and $v_j^r(t)$ at each of the n points on C and at every time step. The second method requires a simulation be run simultaneously with the original problem of Figure 4.4 and therefore the signals $v_j^i(t)$ and $v_j^r(t)$ can be taken directly from the simultaneous simulation. Although this method requires an additional simulation, it is

more efficient than the first method because of the reduced memory storage requirements. In addition, for plane wave excitation the symmetry of the mesh can be utilized to reduce the simultaneous simulation space to a single layer of nodes.

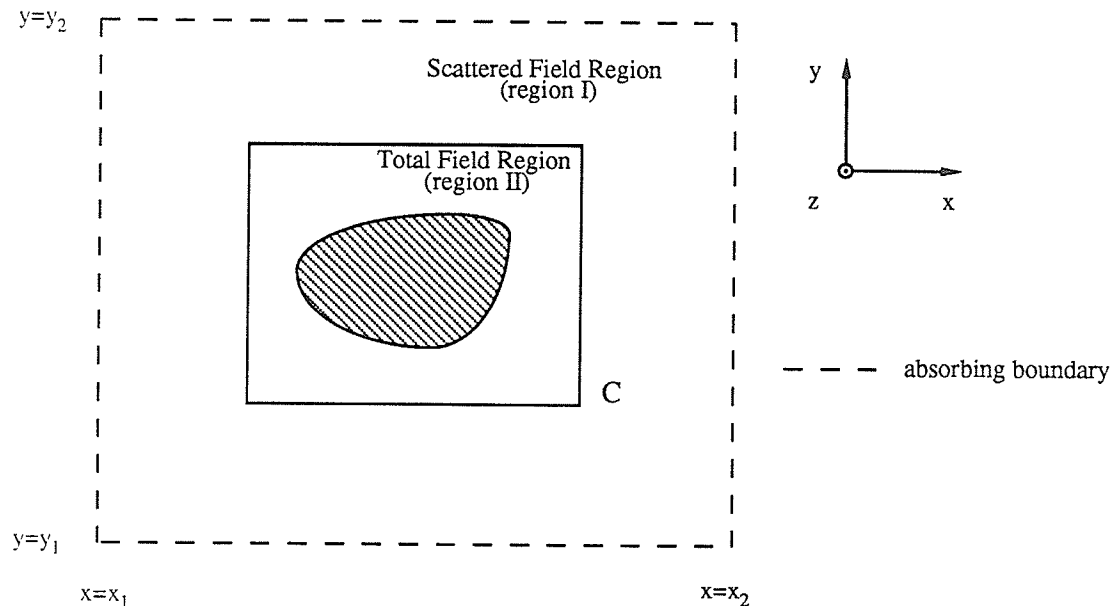


Figure 4.5: TLM simulation space used to model two dimensional scattering problems.

To apply equivalent excitation to Region II with Region I remaining in the simulation space, the operations (i) and (ii) are performed at n points along the contour C and at each time step. A plane wave is generated in Region II with zero fields throughout Region I.

Consider altering Region II by loading nodes with permittivity and conductivity stubs and placing reflection coefficients to model an arbitrary scatterer (as in Figure 4.1). This corresponds to making alterations to the load network L of the original circuit problem. The impulses crossing the contour C from Region II to I no longer

represent the signal $v_j^r(t)$ and non zero impulses are present in Region I. These impulses represent fields caused by the changes made to Region II.

The impulses throughout Region II can be considered as a superposition of original impulses $V_i(x,y,t)$ and a set of impulses produced by the change in network L , $V_\Delta(x,y,t)$. The operations (i) and (ii) allow proper modelling of the impulses $V_\Delta(x,y,t)$ in both regions. Operation (ii) is required to model the impulses $V_\Delta(x,y,t)$ which pass from Region II to I, and operation (i) is required to model the re-reflection of these impulses back into Region II.

The simulation described above can be used to model the scattering problem of Figure 4.1. The impulses $V_i(x,y,t)$ are non zero in Region II only and represent an ideal plane wave. The set of impulses $V_\Delta(x,y,t)$ represent the impulses caused by the placing an object into Region II (or the fields reflected by the object) and are non zero in both regions. Therefore, the set $V_i(x,y,t)$ represents the incident field and the set $V_\Delta(x,y,t)$ represents the scattered field. In Region II the superposition of incident and scattered fields represents the total field and in Region I only the scattered field exists. To properly absorb the outward travelling scattered waves, absorbing boundary conditions are required along the exterior of Region I. The situation described above is shown in Figure 4.5 and represents a general formulation of the TLM method that can be used to model two dimensional scattering problems.

The formulation described above allows illumination of a scatterer by an accurate incident field while applying absorbing boundary conditions to only the scattered fields. The scattered fields are separated from the total fields along the contour C . The only requirement on the placement of C is that all non zero initial conditions are located outside of Region II. The signals representing the incident field used in the operations (i) and (ii) performed along C can be obtained from a simultaneous simulation. The formulation is general in that an arbitrary incident field (not necessarily a

4.2.1. Match Termination of a TLM Mesh

A two dimensional TLM shunt mesh loaded with permittivity stubs represents a medium with characteristic impedance

$$Z_{mesh} = \frac{1}{\sqrt{2 \left[1 + \frac{Y_o}{4} \right]}} \quad (4.1)$$

In the past, to match terminate the mesh a reflection coefficient of

$$\Gamma_{mesh} = \frac{\frac{1}{\sqrt{2 \left[1 + \frac{Y_o}{4} \right]}} - 1}{\frac{1}{\sqrt{2 \left[1 + \frac{Y_o}{4} \right]}} + 1} \quad (4.2)$$

is used to terminate the elemental transmission lines of the model (see Chapter 2 (section 3) and [6]). However the use of (4.2) only provides accurate match termination of the mesh for waves striking the boundary at near normal incidence. If a TLM simulation of waves travelling diagonally through the mesh is considered, the use of (4.2) will cause imperfect matching.

Waves travelling through a unloaded TLM mesh diagonally experience no dispersive effects [6]. Therefore an impulsive plane wave travels as a set of ideal impulses. In this case it is intuitively obvious that a reflection coefficient of zero is required to absorb this wave (this can be verified numerically). Using the reflection coefficient (4.2) would cause non-physical reflections to appear in the TLM simulation space. This contradicts the conclusion regarding match termination of the TLM mesh. A similar example is a plane wave travelling with near grazing incidence to a boundary. Reflection coefficients of approximately 1.0 (magnetic walls) are required along the boundary. As noted by Ney and Yue [40], the reflection coefficient (4.2) does not

provide accurate match termination of the TLM mesh for cases in which near normal incidence is not encountered.

The conflict in reflection coefficients can be resolved by noting that although (4.2) is a mesh quantity, it is applied to the elemental transmission lines which lie along the x and y axes. This termination does provide accurate termination for waves travelling along the x and y axes. However, to absorb waves travelling at an angle ϕ through the mesh, the reflection coefficient (4.2) should be applied in the ϕ direction. Since boundary conditions are enforced by terminating the elemental transmission lines, a modification of (4.2) is required to accurately absorb waves travelling at an arbitrary angle through the mesh.

The required modification to (4.2) can be obtained by examining the propagation of a uniform plane wave through space at an arbitrary angle and the corresponding TLM simulation. In Figure 4.6 an E polarized plane wave propagates in the x - y plane at an angle ϕ to the x axis, in a medium with characteristic impedance Z_o . The electric and magnetic fields associated with this wave are

$$\mathbf{E} = \mathbf{a}_z E_o \quad (4.3)$$

and

$$\mathbf{H} = \mathbf{a}_x H_o \sin\phi - \mathbf{a}_y H_o \cos\phi \quad (4.4)$$

where $Z_o = E_o/H_o$. Along an observation plane located at $x=x_o$ the wave impedance in the x direction is given by [57],

$$Z_x = -\frac{E_z}{H_y} = \frac{Z_o}{\cos\phi} \quad (4.5)$$

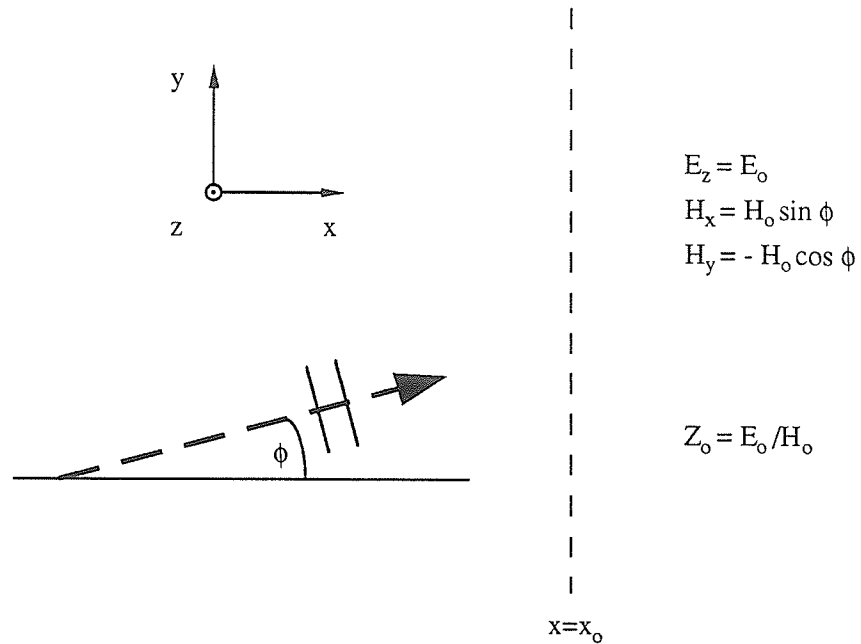


Figure 4.6: *E*-polarized plane wave travelling through space at an angle ϕ to the x axis, crossing the observation plane $x=x_0$.

Consider the corresponding TLM simulation of an E polarized plane wave propagating at an angle ϕ to the x axis in a medium with characteristic impedance Z_0 , but now the above observation plane represents the boundary of the TLM mesh. The wave impedance in the x direction for the plane wave indicates that the mesh should be terminated with

$$Z_{match} = \frac{Z_0}{\cos\phi} \quad (4.6)$$

to achieve a reflectionless termination. This polarization is best represented by a mesh of shunt nodes. A mesh of shunt nodes models a medium of characteristic impedance (4.1) and therefore the voltage reflection coefficient required is,

$$\Gamma_{match} = \frac{\frac{1}{\cos\phi \sqrt{2 \left[1 + \frac{Y_o}{4} \right]}} - 1}{\frac{1}{\cos\phi \sqrt{2 \left[1 + \frac{Y_o}{4} \right]}} + 1} \quad (4.7)$$

Considering an unloaded TLM mesh ($Y_o=0$), this expression fits three angles of propagation for which the proper termination is already known. For normal incidence ($\phi=0^\circ$) the result (4.2) is obtained. At 45° incidence, $\Gamma=0$ agrees with the numerical experiment discussed previously. As well, for $\phi=90^\circ$ (grazing incidence) The expected result of $\Gamma=1$ (a magnetic wall) is obtained from the expression above.

The case of an H polarized wave travelling through the $x-y$ plane at an arbitrary angle ϕ to the x axis can be modelled by a mesh of series nodes. Following the same steps as above the required voltage reflection coefficient for match termination of a series node is given by,

$$\Gamma_{series\ mesh} = \frac{\cos\phi \sqrt{2 \left[1 + \frac{Y_o}{4} \right]} - 1}{\cos\phi \sqrt{2 \left[1 + \frac{Y_o}{4} \right]} + 1} \quad (4.8)$$

Again this fits three angles of propagation for which the reflection coefficient is known ($\phi=0, 45$, and 90 degrees).

Johns and Akhtarzad [21] noted that the voltage scattering matrix for the shunt node is the same as the current scattering matrix for the series node. As expected, in order to achieve match termination, the voltage reflection coefficient for the shunt node is the same as the current reflection coefficient for the series node.

The absorbing boundary condition discussed above will be referred to as the variable impedance absorbing boundary condition, since the impedance value used to

terminate the mesh varies with the angle of incident waves. The implementation of this boundary condition is discussed in the next section.

4.2.2. Implementation of the Variable Impedance Boundary Condition

For plane wave propagation it is easy to see that accurate match termination of the TLM mesh can be obtained at frequencies where the velocity error is negligible. The velocity error and therefore the match termination of the mesh is its worst for axial propagation and at its minimum for diagonal propagation. In an unloaded mesh of shunt nodes simulations were run to determine the reflections caused by (4.2) at normal incidence. Only $\pm 0.3\%$ of the incident wave was reflected indicating extremely good absorption of the incoming waves. Since matching is at its worst for axial propagation, (4.2) would reflect less than $\pm 0.3\%$ for all other angles of incidence (no reflections are introduced for $\phi = 45^\circ$ in a mesh of unloaded nodes).

This condition while theoretically accurate, may not be easily applied to practical problems because the angle of incident waves must be known to apply (4.2). Two methods can be used to implement the variable impedance boundary condition for use in general scattering simulations. The first method is to assume the direction of propagation of the scattered waves incident on the exterior boundary. For simple problems such as scattering from a circular cylinder, a good estimate for the angle ϕ can be made. However, for objects with complex material properties and shapes an estimate for the angle ϕ is not known prior to the simulation. A poor estimate for ϕ would introduce errors into the scattered field results. Therefore, this implementation would only be accurate for cases in which the advance knowledge of the scattered fields is known and is therefore not practical for general scattering simulations. The second method to implement the variable impedance absorbing boundary condition is to use a simple algorithm to estimate the angle of incident waves at each time step using the

field values at nodes adjacent to the boundary. The errors introduced by using this method would be related to the algorithm used to estimate ϕ . This method, while more complicated than the first, lends itself well to implementation in general scattering simulations.

The implementation of either scheme has not been investigated. The first method is limited to simple geometries, and the accuracy of the second method depends on the algorithm used to calculate the angle of incidence. For these reasons practical implementation of the variable impedance boundary condition has not been attempted. Absorbing boundary conditions used in FD-TD simulations of scattering problems have received extensive attention in the literature [3], [49]. The absorbing boundary conditions used in this thesis were originally derived for use with the FD-TD method and have been modified for use with the TLM method. After the work contained in this thesis was completed it came to the author's attention that an absorbing boundary condition using an algorithm to estimate the angle of incidence has been successfully implemented into FD-TD simulations [60]. Therefore it may be worth while to investigate the variable impedance boundary condition in future work.

4.2.3. FD-TD Absorbing Boundary Conditions

A summary of absorbing boundary conditions has been recently presented by Moore *et al* [3]. The paper reviews various absorbing boundary conditions used in FD-TD simulations. A brief summary of the material presented in [3] follows.

Two classes of absorbing boundary conditions are discussed, the first class being *mode annihilating differential operators*. In general the scattered field can be written in spherical coordinates (r, θ, ϕ) as an infinite series of the form [61],

$$U(r, \theta, \phi) = \frac{e^{ikr}}{r} \sum_{n=1}^{\infty} \frac{f_n(\theta, \phi)}{r^n} \quad (4.9)$$

The operators attempt to annihilate as many terms (or modes) as possible in (4.9). The operators are considered as higher order forms of the Sommerfeld radiation condition which eliminates only the first mode of the expansion. This type of boundary condition has not received much attention in electromagnetic field problems.

The second class of absorbing boundary conditions presented are based on approximations to *one way wave equations*. A one way wave equation is a partial differential equation which permits wave propagation in only one direction, and is derived by factoring the multi-dimensional wave equation. The two dimensional wave equation can be written as

$$L U = 0 \quad (4.10)$$

where U is the wave function and the operator L is defined as

$$L = \frac{\partial^2}{\partial x^2} + \frac{\partial^2}{\partial y^2} - \frac{1}{c^2} \frac{\partial^2}{\partial t^2}$$

L can be factored as

$$L = L_x^+ L_x^- \quad (4.11a)$$

or

$$L = L_y^+ L_y^- \quad (4.11b)$$

where

$$L_x^+ = \frac{\partial}{\partial x} - \frac{\partial}{\partial t} \left[1 - \frac{\frac{\partial^2}{\partial y^2}}{\frac{\partial^2}{\partial t^2}} \right]^{1/2} \quad (4.12a)$$

and permits wave propagation in only the positive x direction, and

$$L_x^- = \frac{\partial}{\partial x} + \frac{\partial}{\partial t} \left[1 - \frac{\frac{\partial^2}{\partial^2 y}}{\frac{\partial^2}{\partial^2 t}} \right]^{1/2} \quad (4.12b)$$

and permits wave propagation in only the negative x direction. Similar expressions for L_y^+ and L_y^- can be obtained. Considering a two dimensional simulation of the wave equation (see Figure 4.5) outward travelling waves can be exactly absorbed by placing the operators L_x^+ , L_x^- , L_y^+ , and L_y^- on the boundaries $x=x_2$, $x=x_1$, $y=y_1$ and $y=y_2$ respectively. However, the analytical operators must be discretized by applying difference approximations to the derivatives in (4.12). A significant portion of the work involving the application of absorbing boundary conditions of this class has been involved with higher order approximation to the radical and discretization of the resultant approximation [49].

4.2.4. Higdon's Absorbing Boundary Conditions

The absorbing boundary conditions used in this thesis were developed by Higdon and are formulated for finite difference simulations of the wave equation [62],[63]. The conditions outlined in the previous section are difference approximations to the analytical absorbing boundary conditions for the governing differential equations. Higdon has developed discrete absorbing boundary conditions directly applicable to the difference approximation to the wave equation [62]. A summary of the conditions developed by Higdon follows.

4.2.4.1. General Formulation

Consider the simulation space of Figure 4.5 as a finite difference simulation of a function U that satisfies a two dimensional difference approximation to the two dimensional wave equation. At a location y along the boundary $x=x_1$, and at a time step

$n+1$ an absorbing boundary condition can be expressed in the following form,

$$\mathbf{B} \left[K, Z^{-1} \right] U^{n+1}(x_1, y) = 0 \quad (4.13)$$

where K and Z denote shift operators with respect to the spatial coordinate x and time t respectively and are defined by

$$KU^n(x, y) = U^n(x + \Delta l, y) \quad (4.14a)$$

$$ZU^n(x, y) = U^{n+1}(x, y) \quad (4.14b)$$

The boundary condition $\mathbf{B} \left[K, Z^{-1} \right]$ is an operator that will predict the boundary value of $U^{n+1}(x_1, y)$ using values at previous time steps and spatial positions located inside the simulation space. The following sections outline the two conditions derived by Higdon.

An Averaging Method:

The first condition developed is referred to as *an averaging method*. This type of condition is defined by,

$$\left[I - \left[\frac{I+Z^{-1}}{2} \right] \left[\frac{I+K}{2} \right] \right]^p U^{n+1}(x_1, y) = 0 \quad (4.15)$$

where p is any positive integer, I is an identity operator ($I U^n(x, y) = U^n(x, y)$) and Z and K are the shift operators defined in the previous section. The integer p defines the order of the boundary condition (i.e., a p^{th} order averaging condition). As would be expected higher order conditions provide better accuracy. The first and second order forms ($p=1$ and $p=2$) of the boundary conditions are, respectively,

$$U^{n+1}(x_1, y) = \frac{1}{3} \left[U^{n+1}(x_1 + \Delta l, y) + U^n(x_1, y) + U^n(x_1 + \Delta l, y) \right] \quad (4.16a)$$

$$\begin{aligned}
U^{n+1}(x_1, y) = & \frac{1}{9} \left[\left[6 U^{n+1}(x_1 + \Delta l, y) - U^{n+1}(x_1 + 2\Delta l, y) \right] \right. \\
& + \left[6 U^n(x_1, y) + 4 U^n(x_1 + \Delta l, y) - 2 U^n(x_1 + 2\Delta l, y) \right] \\
& \left. - \left[U^{n-1}(x_1, y) + 2 U^{n-1}(x_1 + \Delta l, y) + U^{n-1}(x_1 + 2\Delta l, y) \right] \right] \quad (4.16b)
\end{aligned}$$

The term averaging arises because the two bracketed terms in expression (4.15) are averages between time steps and space steps respectively.

Space Time Extrapolation:

The second condition developed by Higdon is referred to as *space time extrapolation*. These conditions are defined by,

$$\left[I - Z^{-1}K \right]^p U^{n+1}(x_1, y) = 0 \quad (4.17)$$

The first and second order forms of this condition are, respectively,

$$U^{n+1}(x_1, y) = U^n(x_1 + \Delta l, y) \quad (4.18a)$$

$$U^{n+1}(x_1, y) = 2 U^n(x_1 + \Delta l, y) - U^{n-1}(x_1 + 2\Delta l, y) \quad (4.18b)$$

The term space time extrapolation arises because the field values on the right hand side of the expressions are diagonal patterns in the (x, t) plane. Note that to achieve the same order of approximation p the space time extrapolation conditions require less computation and less storage as compared to the averaging conditions.

4.2.4.2. Stability and Accuracy

To achieve an arbitrarily accurate boundary condition, the value of p could be increased as desired, at the expense of increased storage and computation. For the boundary conditions presented in the previous sections this is not possible. For values $p \geq 3$, the possibility of instability increases. This effect is discussed in detail by Higdon [62]. In practical situations this instability can be ignored because the conditions

for $p=1$ and $p=2$ provide sufficient accuracy.

Both conditions have one-dimensional stencils, meaning that spatial data is only required along a single line perpendicular to the physical boundary. The higher order conditions presented in section 2.3 of this chapter have two dimensional stencils requiring additional spatial data at points along a line parallel to the physical boundary. Conditions that have two dimensional stencils require special treatment in the corners of the mesh increasing the complexity of the implementation. A one dimensional stencil does not imply that only waves at normal incidence to the boundary are absorbed. The conditions have strong multidimensional effects suitable for two and three dimensional simulations under situations with wide angles of incidence. The accuracy of the boundary conditions is demonstrated in the next chapter.

The reflection coefficient R of a p^{th} order boundary condition is,

$$R_p = - \left[\frac{\lambda - \cos\theta}{\lambda + \cos\theta} \right]^p + \mathbf{O} \left[\Delta t \right] \quad (4.19)$$

where $\lambda = \Delta t / \Delta x$, and θ is the angle of incidence measured relative to normal incidence [62]. Higdon considers a boundary condition with reflection coefficient as in (4.19) as providing near perfect absorption for an angle θ which satisfies $\cos\theta = \lambda$. Absorbing boundary conditions have been developed by Higdon which have reflection coefficients of the form,

$$R_p = - \prod_{j=1}^p \left[\frac{\cos\theta_j - \cos\theta}{\cos\theta_j + \cos\theta} \right]^p + \mathbf{O} \left[\Delta t \right] \quad (4.20)$$

and provide perfect absorption at angles $\pm\theta_1, \pm\theta_2, \dots, \pm\theta_p$. Conditions with reflection coefficients of the form (4.20) are consistent with analytical one way wave equations [63]. The conditions used in this thesis are a special case of these boundary conditions ($\theta_1 = \theta_2 = \dots = \theta_p = \lambda$). In the above discussion it is clear that an ideal boundary condition is considered as providing a reflection coefficient of zero for all angles of

incidence. The angles θ_j are chosen to best minimize the reflection coefficient of the boundary condition. The implementation of boundary conditions that have reflection coefficients of the form (4.20) are more complicated than the averaging and space time extrapolation methods and do not have one-dimensional stencils.

The reflection coefficient (4.19) can also be considered as the load reflection coefficient that a wave sees as it approaches the boundary. To match terminate a TLM mesh the variable impedance boundary condition presented in section 2.1 of this chapter can be used. A reflection coefficient (4.2) is applied to the elemental lines of the model. In Chapter 3 it was shown that TLM and FD-TD methods propagate waves in identical manners if the ratio of the time step to the space step is chosen as $1/\sqrt{2}$ in the FD-TD simulation. Substituting $\lambda=1/\sqrt{2}$ into (4.19) and considering the case for $p=1$, the reflection coefficient required to match terminate the TLM mesh is identical to the reflection coefficient that Higdon's boundary conditions present to incoming waves. Therefore Higdon's boundary conditions can be considered as absorbing boundary conditions which automatically satisfy the condition $Z_{match}=Z_o/\cos\theta$, and represent a match termination of the TLM mesh as long as the dispersive nature of the TLM mesh is neglected.

4.2.4.3. Application of Higdon's Conditions to TLM Simulations

In a FD-TD simulation boundary conditions are specified by setting the value of the appropriate field component along the boundary. In the case of applying an absorbing boundary condition the algorithms (4.16) and (4.18) are used to calculate the field component along the boundary. Boundary conditions in a TLM mesh are specified by reflection coefficients along boundaries of the mesh. In the case of absorbing boundary conditions, rather than determine the reflection coefficient at a particular boundary location, the value of the voltage impulse that should be injected back

into the simulation space can be determined. In Figure 4.5, along the boundaries x_1, x_2, y_1 , and y_2 the impulses v_2^i, v_4^i, v_3^i , and v_1^i , respectively, are the unknown impulses that must be injected back into the simulation space at every point on the boundaries and every step in time.

The boundary conditions reviewed in the previous sections are general in that they can be applied to an arbitrary quantity as long as it satisfies a difference approximation to the wave equation.

Consider a general two dimensional electromagnetic field problem with field components E_z , H_x , and H_y present. All of the field components will satisfy the wave equation,

$$\mathbf{W}(E_z) \equiv 0 \quad (4.21a)$$

$$\mathbf{W}(H_x) \equiv 0 \quad (4.21b)$$

$$\mathbf{W}(H_y) \equiv 0 \quad (4.21c)$$

where \mathbf{W} is the two dimensional wave equation operator,

$$\mathbf{W} = \left\{ \frac{\partial^2}{\partial x^2} + \frac{\partial^2}{\partial y^2} - \epsilon \mu \frac{\partial^2}{\partial t^2} \right\} \quad (4.22)$$

In Chapter 3 (section 3.1.2.3) it was shown that a modified TLM scheme is equivalent to the FD-TD method and therefore represents a second order difference approximation to the wave equation. The field components in the mesh therefore satisfy the difference approximation to the wave equation

$$\mathbf{W}_D(E_z) \equiv 0 \quad (4.23a)$$

$$\mathbf{W}_D(H_x) \equiv 0 \quad (4.23b)$$

$$\mathbf{W}_D(H_y) \equiv 0 \quad (4.23c)$$

where \mathbf{W}_D is the difference approximation to the wave equation operator, and E_z , H_x ,

H_y are defined using the modified TLM scheme (Chapter 3 section 3.1.2.2). W_D can be expressed in terms of the spatial shift operators (K_x , for a shift in the x coordinate; and K_y , for a shift in the y coordinate) and the time shift operator (Z), defined in (4.14a) and (4.14b), respectively, as

$$W_D = \left\{ \frac{K_x - 2 + K_x^{-1}}{\Delta l^2} + \frac{K_y - 2 + K_y^{-1}}{\Delta l^2} - \epsilon \mu \frac{Z - 2 + Z^{-1}}{\Delta t^2} \right\} \quad (4.24)$$

In a TLM mesh of unloaded nodes, impulses incident upon a node at a particular time step, scatter off the transmission line junction, and become incident impulses on adjacent nodes at the next time step. Therefore, at any time step, sets of incident impulses on adjacent nodes are independent.

Consider two adjacent nodes in a TLM mesh of unloaded shunt nodes located at (x, y) and $(x + \Delta l, y)$. Using the modified TLM scheme to define the magnetic field, H_y can be defined at $(x + \Delta l / 2, y)$ in terms of the impulses on the elemental transmission lines as,

$$H_y(x + \Delta l / 2, y) = v_2^i(x + \Delta l, y) - v_4^i(x, y) \quad (4.25)$$

where $v_2^i(x + \Delta l, y)$ denotes an incident impulse on branch 2 of the node located at $(x + \Delta l, y)$ and $v_4^i(x, y)$ denotes an incident impulse on branch 4 of the node located at (x, y) . Substituting (4.25) into (4.23c), yields,

$$W_D(v_2^i(x + \Delta l, y) - v_4^i(x, y)) \equiv 0 \quad (4.26)$$

The two impulses in (4.26) are incident impulses on adjacent nodes and are therefore independent. Therefore, each impulse must independently satisfy $W_D(\) \equiv 0$,

$$W_D(v_2^i(x + \Delta l, y)) \equiv 0 \quad (4.27a)$$

$$W_D(v_4^i(x, y)) \equiv 0 \quad (4.27b)$$

Since the positions of the two adjacent nodes in the mesh is arbitrary, the impulses

incident on branches 2 and 4 will always satisfy $W_D(\cdot) \equiv 0$. Similarly, examining two nodes adjacent in the y direction (and using the definition of H_x), impulses incident on branches 1 and 3 will always satisfy $W_D(\cdot) \equiv 0$. The above argument proves that the individual impulses travelling on the elemental transmission lines satisfy the difference approximation to the wave equation. Therefore the operations (4.16) and (4.18) can be applied to predict future values of the voltage impulses that should be injected back into the simulation space.

4.3. Calculation of Far Field Patterns

Accurate absorbing boundary conditions allow the simulation space to be truncated to within a small distance from the scatterer which is in the near field region. Although this allows the method to be computationally efficient, this disallows obtaining the scattered far field distributions directly from output points within the simulation space. A method is required to calculate the far field distributions from the data available from the simulation. Three methods are presented and all use equivalent sources to calculate the scattered fields in the far field region. The first method uses the surface currents on the scatterer as the sources of the scattered field. The second method uses the near scattered fields to obtain equivalent sources for the scattered field in the far field region. The third is similar to the second, but it operates in the time domain rather than the frequency domain.

4.3.1. Surface Current to Far Field Transformation

Considering only the case of TM scattering, an object of arbitrary media properties has electric and magnetic currents (J_z and $M_{x,y}$ respectively) flowing on its surface. These currents are the physical sources of the scattered field and can therefore be

used to calculate the scattered field at any point in space. The magnetic and electric vector potentials at a point (ρ, θ) in the far field can be calculated using [57]

$$A_z(\rho, \phi) = \frac{e^{-jk\rho}}{\sqrt{8j\pi k\rho}} \iint_{S'} J_z(\rho') e^{jk\rho' \cos(\phi - \phi')} ds' \quad (4.28)$$

and

$$F_{x,y}(\rho, \phi) = \frac{e^{-jk\rho}}{\sqrt{8j\pi k\rho}} \iint_{S'} M_{x,y}(\rho') e^{jk\rho' \cos(\phi - \phi')} ds' \quad (4.29)$$

respectively where S' corresponds to the surface of the scatterer and (ρ', ϕ') is a point on the surface, and k is the wave number at a particular frequency. The electric field at any point in space can be obtained from the magnetic and electric vector potential using,

$$E_z = -j\omega\mu A_z + jk(F_x \cos\phi - F_y \sin\phi) \quad (4.30)$$

The electric and magnetic surface current distributions can be determined from the relations $J_z = \hat{n} \times H_{x,y}$ and $M_{x,y} = -\hat{n} \times E_z$ where \hat{n} is the outward pointing unit vector normal to the surface of the scatterer. Boundaries in TLM simulations are defined at locations half way between nodes and field quantities are defined at nodes. The values of the electric and magnetic fields (to calculate the magnetic and electric currents respectively) available from the TLM algorithm are located half a mesh spacing away from the surface of the scatterer. Because of this an assumption that the field will not change significantly over half a mesh spacing is required. In general this assumption is valid because over the frequency range of interest half a mesh spacing is a small fraction of a wavelength. However, when considering scatterers with corners or edges such as rectangular cylinders, the fields change rapidly in the vicinity of the corner or edge because of the singularity in the field distribution. Near these singularities the above assumption is false and as a result the surface current distributions is not accurate. In addition, for arbitrarily shaped scatterers output points must be reconfigured for each

change in the geometry of the scatterer.

4.3.2. Near Field to Far Field Transformation

A more general and more accurate method is to use the scattered near fields as the source of the scattered far fields. Output points are placed along a contour S' in the scattered field region as shown in Figure 4.7. Because output points are not placed on the surface of the scatterer the near-to-far field transformation eliminates the problems associated with the surface current to far field transformation for modelling problems with singularities in the field distributions.

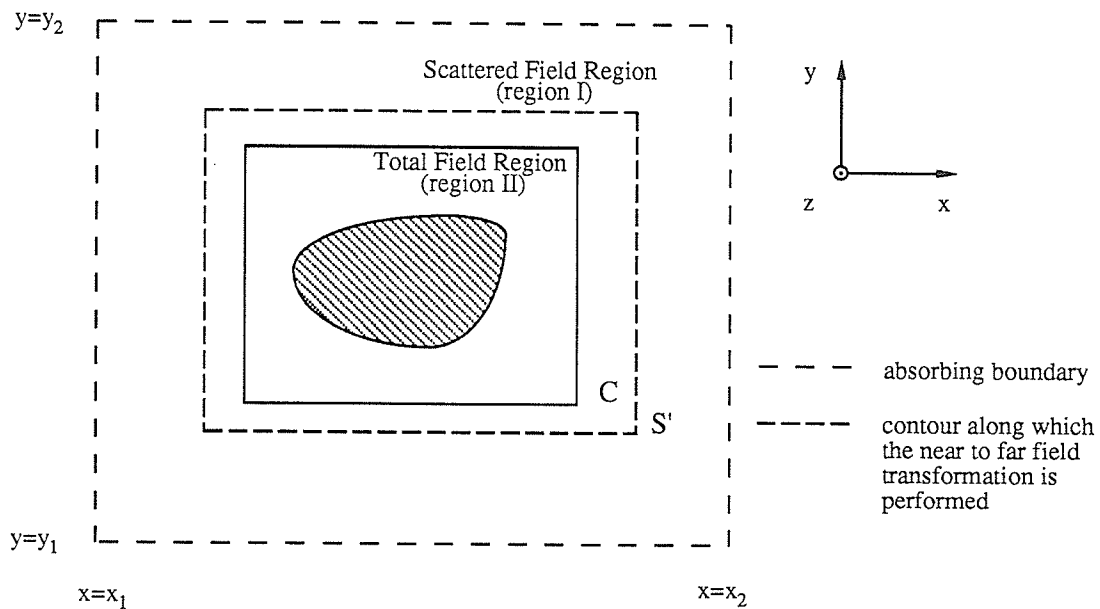


Figure 4.7: TLM simulation space used to model two dimensional scattering problems with the contour S' along which the near- to-far field transformation is performed.

Along the surface S' , equivalent electric source current J_z^e and the equivalent magnetic source current $M_{x,y}^e$ are obtained from the scattered magnetic and electric

fields, respectively. The scattered far field is calculated using expressions (4.28-4.30).

4.3.3. Direct Transformation to the Far Field in the Time Domain

The two transformations presented in the previous sections are frequency domain transformations. The TLM method operates in the time domain and therefore the time domain results must be Fourier transformed before far field results can be calculated. Recently, a method has been presented [64],[60] to extrapolate time domain scattered fields directly to the far field without first Fourier transforming to the frequency domain. The time domain far fields are then Fourier transformed to obtain frequency domain far fields. The method is identical to the near-to-far field transformation presented earlier except the transformation is performed in the time domain. For the two dimensional TM scattering problems considered in this thesis the electric field is obtained by evaluating

$$E_z(\hat{r}, t) = -\frac{\mu}{4\pi} \int \hat{r} \times \left\{ \frac{\partial J_z^e(\hat{r}', t-\tau)}{\partial t} \times \hat{r} \right\} dS' - \frac{1}{4\pi c} \int \frac{\partial M_{x,y}^e(\hat{r}', t-\tau)}{\partial t} \times \hat{r} dS' \quad (4.31)$$

where \mathbf{r} represents the observation point (ρ, ϕ) and $\tau = t - r/c$. The method became known to the author at the time of writing this thesis and implementation or testing has not been possible.

4.3.4. Calculation of Frequency Domain Scattered Fields from Time Domain Field Simulations

The goal of this thesis is to investigate the use of the TLM method to simulate scattering problems. The TLM method operates in the time domain, therefore sinusoidal excitation or pulse excitation and Fourier transformations are required to

obtain frequency domain results. Three methods are outlined to obtain frequency domain far fields from a time domain simulation.

Method 1:

In the past, sinusoidal excitation has been used to illuminate the scatterer and the algorithm has been run to a near steady state condition (requiring 2-3 cycles of the incident wave). One of the frequency domain far field transformations presented in the previous two sections is then used to calculate the scattered far fields at the excitation frequency. This scheme requires no Fourier transformations but for each new frequency the entire field simulation and a transformation to the far field is required. The relative cpu time required to obtain results at N_f frequency points is

$$\text{cpu time}_1 \propto N_f T_{sim}^f + N_f N_{FF} T_{N \rightarrow F}^f \quad (4.32)$$

where T_{sim}^f is the time required to perform a TLM simulation with sinusoidal excitation, N_{FF} is the number of far field observation points, and $T_{N \rightarrow F}^f$ is the time required to perform a frequency domain near-to-far field transformation.

Method 2:

A second method to obtain frequency domain far fields is to use a pulse excitation from which a single simulation and multiple Fourier transformations at the output points will yield frequency domain near scattered fields or surface currents. At each frequency a far field transformation is required. The relative cpu time required to obtain results at N_f frequencies is

$$\text{cpu time}_2 \propto T_{sim}^t + N_f N_{S'} T_{F.T.} + N_f N_{FF} T_{N \rightarrow F}^f \quad (4.33)$$

where T_{sim}^t is the cpu time required to perform a TLM simulation with pulse excitation, $N_{S'}$ is the number of output points along the contour S' , and $T_{F.T.}$ is the time required to perform a Fourier transformation. The times T_{sim}^t and T_{sim}^f are approximately the same [5]. Note that the cpu time required to perform a single Fourier

transformation or a near-to-far field transformation is much less than the time required to perform the TLM simulation. For this reason this method is more efficient than Method 1 above. The cpu time required for Method 1 is approximately a linear function of N_f while the cpu time required for Method 2 increases only slightly with N_f . If Method 2 is used to obtain frequency domain far fields the efficiency of the TLM method approaches that of the Boundary Element Method if results over a wide bandwidth are required.

Method 3:

The previous two methods use the frequency domain far field transformations presented in section 3.1 and 3.2 of this chapter. The third method presented uses the time domain near-to-far field transformation presented in section 3.3 of this chapter. A pulse is used as excitation and the time domain fields along the contour S' are used directly in the near-to-far field transformation. At each observation point in the far field a Fourier transformation is required to calculate the frequency domain scattered fields. The cpu time required to obtain results at N_f frequencies is

$$\text{cpu time}_3 \propto T_{sim}^t + T_{N \rightarrow F}^t + N_f N_{FF} T_{F.T.} \quad (4.34)$$

where $T_{N \rightarrow F}^t$ is the time required to perform a time domain near-to-far field transformation. Depending on the number of far field observation points and the number of points along the contour S' this method may or may not be more efficient than Method 2. Note that N_f frequency domain near-to-far field transformations are required for Method 2 while only one time domain near-to-far field transformation is required in this method. The time domain near-to-far field transformation requires significantly more cpu time and memory storage than the frequency domain near-to-far field transformation. As previously mentioned the time domain near-to-far field transformation became known to the author at the time of writing this thesis. Comparing the accuracy and efficiency of this method to Method 2 has not been investigated.